

~~CONFIDENTIAL~~

Copy 311  
RM E56L04

144 55  
JUL 31 1957

TECH LIBRARY KAFB, NM  
0143989

NACA RM E56L04

6997

**NACA**

# RESEARCH MEMORANDUM

ARRANGEMENTS OF JET ENGINE AND AIRFRAME FOR  
INCREASED RANGE

By Roger W. Luidens

Lewis Flight Propulsion Laboratory  
Cleveland, Ohio

Classification (or change to *Unclassified*)  
By *NASA Tech Pub Announcement #4*  
(or change to change)

By *16 Mar. 59*

*NK*

GRADE OF OFFICER MAKING CHANGE)

*14 Mar. 61*  
DATE CLASSIFIED DOCUMENT

This material contains information affecting the National Defense of the United States within the meaning of the espionage laws, Title 18, U.S.C., Secs. 793 and 794, the transmission or revelation of which in any manner to an unauthorized person is prohibited by law.

**NATIONAL ADVISORY COMMITTEE  
FOR AERONAUTICS**

WASHINGTON

July 26, 1957

~~CONFIDENTIAL~~



## TABLE OF CONTENTS

	Page
SUMMARY . . . . .	1
INTRODUCTION . . . . .	1
ANALYSIS AND DISCUSSION . . . . .	2
Inlet Location to Reduce Inlet Momentum . . . . .	2
Inlet Location to Increase Inlet Pressure Recovery . . . . .	4
Jet Cant for Lift (Inlet in Free Stream) . . . . .	5
Combined Effect of Inlet Location and Jet Cant for Lift . . . . .	6
Engine Moments for Trim . . . . .	7
Combined Effect of Inlet Location, Jet Cant for Lift, and Jet Offset for Trim . . . . .	9
Use of Boundary Layer in Engine . . . . .	10
CONCLUSIONS . . . . .	12
APPENDIXES	
A - SYMBOLS . . . . .	14
B - BASIC CONSIDERATION OF THE RANGE EQUATION . . . . .	18
C - DETERMINATION OF CRUISE LIFT COEFFICIENT, ANGLE OF ATTACK, LIFT-DRAG RATIO, AND RATIO OF FRICTION DRAG TO TOTAL DRAG . . . . .	20
D - EQUATIONS INTERRELATING SEVERAL ENGINE PARAMETERS . . . . .	24
E - EFFECT ON RANGE OF ENGINE-INLET MOMENTUM REDUCTION DUE TO AIRFRAME PRESSURE DRAG . . . . .	26
F - EFFECT ON RANGE OF AN INCREASE IN PRESSURE RECOVERY DUE TO INLET LOCATION . . . . .	31
G - EFFECT ON RANGE OF EXHAUST-JET CANT FOR LIFT . . . . .	32
H - EFFECT ON RANGE OF TRIM DRAG . . . . .	38
Conventional Fixed Tail . . . . .	38
Fixed Canard . . . . .	40
Fixed-Floating Canard . . . . .	42
I - JET CANT FOR AIRPLANE TRIM . . . . .	44

	Page
J - MOMENTS DEVELOPED BY ENGINE INTERNAL FLOW FOR TRIM . . . . .	45
Case I . . . . .	46
Case II . . . . .	46
Case III . . . . .	47
K - EFFECT ON RANGE OF USING AIRFRAME BOUNDARY LAYER IN ENGINE .	48
REFERENCES . . . . .	53
FIGURES . . . . .	55

~~CONFIDENTIAL~~

## NATIONAL ADVISORY COMMITTEE FOR AERONAUTICS

RESEARCH MEMORANDUM

## ARRANGEMENTS OF JET ENGINE AND AIRFRAME FOR INCREASED RANGE

By Roger W. Luidens

## SUMMARY

A number of factors affecting engine-airframe arrangements are evaluated in terms of range. All the effects considered are related to the engine internal flow. Appropriate equations are developed and evaluated for flight Mach numbers from 1.0 to 5.0, for ram-jet and turbojet engines with cycle temperatures from 2500° to 3500° R, and for airplane lift-drag ratios of 4 and 8. The following are examples of the calculated results at a flight Mach number of 4.0 for a ram jet with a maximum cycle temperature of 3500° R, for an airplane with a lift-drag ratio of 4. Locating the engine inlet under the wing increases range 16 percent. Canting the exhaust jet for lift to the optimum angle increases range about 9 percent. Using internal engine moments to avoid trim drag may increase range by 8 percent. Using airframe boundary layer in the engine cycle shows possible theoretical gains in range of about 17 percent.

## INTRODUCTION

This report discusses, from the point of view of the propulsion system, some of the arrangements of the engine with respect to the airplane that will yield increased airplane range. All the effects discussed are related to the engine internal flow. The factors of engine arrangement considered are inlet location, jet cant, use of engine moments for trim, and use of boundary layer in the engine. The purpose of the report is then twofold: (1) to develop the appropriate equations, and (2) to evaluate these equations for several values of the involved parameters to establish orders of magnitudes and trends. The quantitative results are presented as percent change in airplane range as a function of flight Mach number for two values of airplane lift-drag ratio and for two engine cycle temperatures.

A number of the ideas evaluated in this report have been previously discussed (e.g., ref. 1) but not evaluated in terms of airplane range. The developments and engine performance of reference 2 are a background and basis for the present work.

~~CONFIDENTIAL~~

4077

CL-1

## ANALYSIS AND DISCUSSION

The following approach is taken in the analysis. A reference airplane illustrated in figure 1 is assumed, and the effect of making changes from the configuration is calculated. The airplane components such as the wing, fuselage, and engine remain fixed in size, only their arrangement being changed. This approach avoids the problem of having to evaluate weight changes. The exact arrangement of the reference airplane will be made clear in the course of discussing modifications to it. Percent increase in airplane range is the quantitative measure of performance used in the analysis. Other airplane features are mentioned qualitatively.

The detailed mathematical developments of the analysis are presented in the appendixes. Basic to most of the analysis is the assumption of small changes. When the calculated changes in range become large, their precision degenerates. Of course, large changes are the interesting ones. Thus, the accuracy of large gains may be in question, but the trends are correct. The symbols used are given in appendix A, and the mathematical approach to the range equations is discussed in appendix B.

The body of the report explains principles and discusses numerical results from the analysis. For most of the calculations, a turbojet cycle having a 2500° R turbine-inlet temperature was used below Mach 3.0 and a ram-jet cycle above Mach 3.0. The curves are in general plotted from  $M = 1.0$  to 5.0, for engine cycle temperatures of no afterburning for the turbojet, 2500° R final temperature for the ram jet, and for 3500° R final temperature for both. Airplanes with maximum lift-drag ratios of 4 and 8 are evaluated. Airplane modifications are discussed in the following order: inlet locations to reduce inlet momentum, inlet location to increase pressure recovery, jet cant for lift, engine moments for trim, and use of boundary layer in the engine cycle.

## Inlet Location to Reduce Inlet Momentum

Locating the inlet on the airplane to obtain increased range is considered first. The following two effects are treated analytically: (1) the effect of locating the inlet to reduce inlet momentum, and (2) the effect of locating the inlet to increase inlet pressure recovery. The detailed mathematical development of the effect on range of inlet location to reduce inlet momentum is given in appendix E. The basic concepts and results are summarized here.

The conventional definition of thrust (and the thrust defined by the engine manufacturer) is the exit momentum minus the inlet momentum in the free stream. (Note that in the reference airplane configuration

the inlet is in the free stream.) If the inlet is located in the vicinity of a body with a drag that exists without the presence of the engine, the local stream momentum  $\Phi$  at the inlet is less than the free-stream momentum, and the thrust of the engine is effectively greater than that defined by the manufacturer. (Alternatively, the airplane drag can be considered to be effectively reduced.) For example, for a two-dimensional flat-plate wing at angle of attack, the momentum of a stream tube of air under the wing decreases below the free-stream value and the local Mach number also decreases. On the upper side of the wing, the momentum of a stream tube of air also decreases, but in this case the local Mach number has increased above the free-stream value. According to this discussion, the inlet could be located to advantage almost anywhere in the influence of the airframe.

One of the more interesting locations for the inlet is under a lifting surface; for example, under a wing (illustrated in fig. 2), where it can take advantage of the momentum reduction due to both wing angle of attack and thickness. Such a case has been evaluated as a function of flight Mach number for two engine cycle temperatures, and the results are presented in figure 3. The engine cycle temperature is the maximum temperature that exists in the engine cycle before a change is made to the airplane. According to the developments in appendix D of reference 2, if the airplane altitude is assumed to be the same before and after a change, then the cycle temperature must change somewhat. However, if the airplane altitude is allowed to vary, then the engine cycle temperature can be kept constant. Either assumption yields the same result for the range gain. The wing was assumed to have a thickness ratio of 4 percent and a diamond profile. The wing angle of attack is determined by the airframe lift-drag ratio, the engine cycle temperature, and the condition that the airplane is flying at the maximum product of lift-drag ratio and engine specific impulse, for maximum range. The relations determining the wing angle of attack are developed in appendix C. Calculations are presented for two airplane maximum lift-drag ratios  $(L/D)_{\max}$ . The airplane cruise lift-drag ratio  $L/D$  is slightly less than the maximum lift-drag ratio. The relation of the cruise-to-maximum lift-drag ratio is also given in appendix C.

Figure 3 shows that the range importance of inlet location increases with increasing flight Mach number. For example, at  $M = 1.0$  the gain in range is less than 1.2 percent for all the conditions considered. At Mach 4.0 for an airplane with a lift-drag ratio of 4 cruising at  $3500^{\circ} R$ , a 5.7-percent range gain can be realized, and larger gains exist for lower cycle temperatures. A qualification is necessary here. The range results in this section and in subsequent sections above  $M = 3.4$  at  $2500^{\circ} R$  and above  $M = 4.6$  at  $3500^{\circ} R$  engine cycle temperature have practical significance only if for some reason these temperatures are the maximum permissible engine cycle temperature. The reason is explained in appendix C. Therefore, this portion of the curves is dashed.

In general, the available gains increase with decreasing cycle temperature and decreasing airplane lift-drag ratio. The effect of lift-drag ratio and cycle temperature may be understood from the principle that factors that increase the quantity of air handled by the engine compared with that handled by the wing increase the importance of inlet momentum reduction. Thus, decreasing lift-drag ratio and decreasing cycle temperature both increase the required airflow through the engine and hence the importance of inlet location. The preceding calculation was made assuming no change in inlet pressure recovery (total pressure at the compressor face or in the combustor divided by free-stream total pressure) with inlet location. It was also assumed that the lift of the configuration is not affected by locating the inlet under the wing.

#### Inlet Location to Increase Inlet Pressure Recovery

If the local Mach number ahead of the inlet is isentropically decreased, then an increase in the attainable inlet total-pressure recovery (defined here as the total pressure of the diffuser discharge divided by the free-stream total pressure) may logically be expected. Appendix F presents the mathematical relation of inlet location to pressure recovery and range, as well as the assumed variation of pressure recovery with Mach number. In the previous discussion of inlet momentum, momentum decreases associated with local Mach number increases or decreases were equally acceptable. However, when consideration is also given to obtaining high pressure recovery, the locations that yield reduced Mach numbers are more desirable. Inlet locations under a lifting surface and under the nose of the fuselage satisfy these requirements. By potential-flow theory, reduced Mach numbers also exist on the aft converging areas and downstream of axisymmetric bodies. Again, the case of an inlet under the wing as compared with the inlet in the free stream is calculated for an example. Whether in the free stream or under the wing, the inlet itself is assumed to yield the best pressure recovery available from an inlet designed for the local Mach number, and having two oblique shocks and a normal shock. The total-pressure loss through the shock generated by the wing as well as the Mach number reduction is accounted for. The results of such a calculation are presented in figure 4. The gain at  $M = 1.0$  is zero because the inlet pressure recovery is assumed independent of Mach number for  $M$  less than 1.0. At  $M = 4.0$  for an airplane with a maximum lift-drag ratio of 4 (fig. 4(a)), the gain in range is 10.7 percent at a cycle temperature of  $3500^{\circ}$  R. In general, the effect of airplane lift-drag ratio is in the same order as previously discussed. The effect of cycle temperature, however, is in the opposite order. This calculation has been made assuming the inlet momentum to be the free-stream value. Thus, the gains due to pressure-recovery increase and inlet-momentum decrease as calculated are additive. The result of this addition, presented in figure 5, represents the total effect of inlet location. For example, at  $M = 4.0$  for an airplane with a maximum  $L/D$  of 4, the effect of inlet location on range is about 16.5 percent at  $3500^{\circ}$ . The effect of engine cycle temperature is quite small.

The gain by putting the inlet under the wing is considered in this section. Appendix H shows that, for a canard airplane arrangement, the canard angle of attack at supersonic speeds may be 2 or 3 times that of the wing. If the pressure field of the canard can be effectively used, the range gains may well be larger than those shown for putting the inlet under the wing.

4011

Other gains may be realized by locating the inlet under the wing or nose of the fuselage. One of these is that the direction of the inlet airflow is independent of airplane angle of attack. A change in airplane angle of attack results only in a change in local Mach number ahead of the inlet. The inlet can usually more readily adapt itself to a Mach number change than to a change in flow direction. Also, by locating the inlet in a region of favorable compression, the maximum Mach number for which the inlet must be designed may be reduced. This is important to the design of the inlet for engine-inlet matching.

#### Jet Cant for Lift (Inlet in Free Stream)

Lift obtained by canting the exhaust jet downward as illustrated in figure 6 can be used to obtain increases in range. This effect is developed in detail in appendix G. In the reference airplane (fig. 1) the exhaust jet (as well as the net thrust vector) is aligned with the free-stream or flight direction.

The exhaust momentum changes in the lift and thrust directions with the sine and cosine of the angle of cant, respectively. Hence, a small angle of exhaust-jet cant below the flight direction results in an increment of lift but practically no loss in thrust. This increment of lift obtained from the jet is no longer carried by the wing, and the airplane drag due to lift is consequently slightly reduced. The engine can now be throttled back slightly, and a range increase generally results. Clearly, at high angles of jet deflection appreciable thrust losses exist, and range losses will occur. Figures 7 and 8 present percent range improvement as a function of the angle of exhaust-jet cant. The range increases for angles of downward cant greater than zero (the reference condition is that of zero cant), reaches a peak, and then decreases for each case. The circle symbols are at the peak of curves as determined by a separate calculation.

It is interesting to compare the angle of jet cant with the wing angle of attack. If the airplane is flying at  $[(L/D)I]_{\max}$  and the airframe maximum lift-drag ratio and the engine cruise cycle temperature are known, the wing angle of attack is determined (see appendix C). A triangular symbol is placed on the curves where the angle of jet cant is equal to the wing angle of attack. The optimum angle of jet cant (circle symbol) is always twice the wing angle of attack. This may also be seen

by comparing equations (G11) and (G34). However, more than half of the available range gain from jet cant is achieved by canting the jet to the same angle as the wing. Of course, if the engine is at zero incidence with respect to the wing, this gain results naturally. The range improvement for the optimum angle of jet cant is cross-plotted as a function of flight Mach number for two airplane lift-drag ratios and two engine cycle temperatures in figure 9. Again, the range importance of jet cant increases with increasing flight Mach number. At  $M = 4.0$ , for example, the range gain for an airplane with a maximum lift-drag ratio of 4 is 8.8 percent for engine cruise cycle temperature of  $3500^{\circ}$  R. The gain is greater for lower cycle temperatures and less for higher lift-drag ratios.

The effects of lift-drag ratio and cycle temperature are in the order determined by the ratio of exit momentum to airplane gross weight. That is, low lift-drag ratio and low cycle temperature both increase the size of the exit momentum compared with airplane gross weight and result in increased importance of jet cant. This order is the same as that previously observed with respect to inlet location for decreased inlet momentum.

#### Combined Effect of Inlet Location and Jet Cant for Lift

Under the assumption that the configuration external lift is not changed by placing the inlet under the wing, the effects of inlet location and jet cant for lift with the inlet in the free stream are additive as calculated even though the inlet is under the wing. If, however, to keep the lift of the configuration constant, a downward cant of the exhaust jet is required (i.e., to conserve the downward momentum of the air deflected by the wing), then the effect of jet cant for lift is modified. Under this assumption, the additional advantage of jet cant for lift is somewhat reduced although the best angle of jet cant remains the same. The angle of jet cant to conserve the downward momentum (associated with lift) of the air entering the inlet is shown in figures 7 and 8 as the square symbols. The available range gain from optimum jet cant is then the difference between the values at the circle and square symbols. This is illustrated graphically in figure 7(f).

Consider two examples at  $M = 4.0$  for an airplane having a maximum lift-drag ratio of 4 and an engine cycle temperature of  $3500^{\circ}$  R. The addition of the separate effects of inlet location under the wing and canting the exhaust jet to its optimum value gives a range gain of 25.3 percent. This corresponds to the first assumption mentioned above. Using the second assumption mentioned above gives a range gain of 18.1 percent. This result was obtained using equation (E25), the results shown in figure 4, and the reduced range gain shown in figure 7(f).

## Engine Moments for Trim

4077

Moments from the engine internal flow may be used to trim the airplane and in many cases with a consequent improvement in range. The problem of trim drag applies primarily to airplanes that are required to fly at both subsonic and supersonic speeds. Consider a conventionally arranged airplane that is designed for tail-off neutral static longitudinal stability at subsonic speeds (fig. 10(a) and the reference airplane of fig. 1). When the airplane flies to supersonic speeds, the airplane center of lift shifts rearward, resulting in a nose-down moment about the airplane center of gravity. For the conventionally arranged airplane (tail aft of the wing), this moment must be counteracted by a down load on the tail. The down load on the tail must in turn be supported by lift on the wing. The sum of the drags resulting from the shift in center of lift is termed the trim drag.

The effect of trim drag on airplane range for a conventional and several canard airplane arrangements (illustrated in fig. 10(b)) is developed in appendix H. There are several ways that the engine moments can be used to avoid or reduce the trim drag. If the engine exhaust is at the rear of the airplane, as illustrated in figure 11, the jet may be canted upward to develop the required down force. (This is of course inconsistent with obtaining lift from the jet by canting it downward as previously discussed.)

The effect on airplane range of canting the jet for trim is developed in appendix I. Figure 12 compares the range gain (note that the gain is negative, hence a loss in range due to trim drag) for several methods of trimming an airplane and for two values of  $c/t$ . A value of  $c/t = 0.05$ , for example, means that the tail moment arm is 20 times the center-of-pressure shift. Each airplane is defined to have the same margin of static stability at subsonic speeds, the same wing and tail (or canard) areas, and the same moment arms. The losses in range due to trim drag depend directly on the wing center-of-pressure shift  $c$  and the tail moment arm  $t$ . The curves where a tail or canard surface is used for trim were essentially independent of airplane lift-drag ratio and engine cruise cycle temperature, although this is not obvious from the equations. However, when the exhaust jet is used for trim, both the angle of jet deflection and the range gain depend on the airplane lift-drag ratio and the engine cycle temperature. The loss in range for trimming with exhaust-jet cant increases with increasing flight Mach number and decreasing engine cycle temperature. These two losses are in the same order as the gains due to using jet cant for lift. However, the loss in range due to trimming with the exhaust jet for airplanes with high lift-drag ratios is larger than for airplanes with low lift-drag ratios. This is the opposite order observed for the gain due to jet cant for lift.

Of the airplanes trimmed with a tail, the conventional and fixed-canard airplane arrangements show the greatest and about the same trim-

drag effect on range (fig. 12). This loss in range is about 8 percent for an airplane with  $(L/D)_{\max}$  of 4 and  $c/t$  of 0.05. The canard arrangement where the canard is free floating at subsonic speeds and fixed at supersonic speeds shows a smaller range reduction due to trim drag. Using the exhaust jet to trim causes a still smaller range loss than a fixed-floating canard below about  $M = 2.7$  for most of the examples calculated. It is implied that using the exhaust jet for trim requires a jet that can be swiveled, canted, or deflected by vanes in flight. If the moment generated at subsonic speeds is small or designed for, the nozzle can be designed at a fixed angle, as will be discussed subsequently. Also, the range losses shown here for jet cant for trim do not consider the forfeiting of the gain that might otherwise be had from canting the jet downward for lift.

There are other ways of utilizing the moments developed by the engine internal flow to avoid trim drag without requiring variable deflection of the exhaust jet and at the same time retaining all or some of the gains discussed under "inlet location" and "jet cant for lift." The required mathematical relations are developed in appendix J. When the airplane flies to supersonic speed, the drag, and hence the thrust, increases. Because the center-of-lift shift and thrust increase are concomitant, the engine can be arranged on the airplane so that the tail-off moments about the airplane center of gravity are zero at both subsonic and supersonic speeds and the trim drag thus avoided. Three special arrangements for avoiding trim drag are illustrated in figure 13. The first uses the thrust vector (exit momentum minus inlet momentum). The second uses only the inlet momentum. The exit momentum vector passes through the center of gravity. The third case uses only the exit momentum, and the inlet is located at the airplane center of gravity. This latter case has the advantage that the exit momentum is a larger vector than either the inlet momentum vector or the thrust vector and will consequently require the least offset.

Figure 14 presents the amount of offset as a fraction of the center-of-lift shift, required to avoid trim drag, as a function of airplane  $L/D$  and engine cycle temperature. To avoid the problem of having to define the subsonic airplane  $L/D$  and engine operating condition, these calculations have been made for the limiting case of  $(L/D)_b = \infty$ . Many of the offsets shown, particularly at the lower flight Mach numbers, may be larger than can be conveniently incorporated in an airplane configuration. By using one of these ways of avoiding trim drag, the range loss for trimming the airplane with a lifting surface (fig. 12) can be avoided. The size of the offset for the three cases follows the order previously discussed. The effects of cycle temperature and airframe lift-drag ratio are again in the order of the ratio of inlet or exit momentum to the air-flow handled by the wing. Thus, lower lift-drag ratios and lower cycle temperatures reduce the required offset to avoid trim drag.

It should be pointed out that there are other techniques for avoiding trim drag, such as cambered and reflexed fuselages and shifting

internal weight (such as fuel) within the airplane to reduce the moment about the center of gravity.

Combined Effect of Inlet Location, Jet Cant for  
Lift, and Jet Offset for Trim

Of course it is of interest to add together the effects discussed so far and to see what they mean in terms of the airplane configuration. Two combinations that are distinguished by the method used to avoid trim drag are considered. The first combination uses the method illustrated in figure 13(c), case III. The second combination uses the method illustrated in figure 11. The results of combining the advantages of inlet location under the wing, jet cant for lift, and avoiding trim drag by using offset of the exit jet (as illustrated by case III, fig. 13(c)) are presented in figure 15. In this figure the trim drag saved is conservatively assumed to be that for the floating-fixed canard for tail moment arm 20 times the center-of-pressure shift from subsonic to supersonic speeds ( $c/t = 0.05$ ). As a representative value of the other effects, the results for the inlet under the wing shown in figure 3 were added to the range gain due to jet cant for lift between the optimum angle of jet cant and the angle of cant to conserve configuration lift. The combined effect increases with increasing flight Mach number, with decreasing cycle temperature, and decreasing airframe  $L/D$ , as have most of the individual effects. At Mach 4.0 for an airplane with a maximum  $L/D$  of 4, the percent increase in range is 25.6 percent for a cycle temperature of 3500° R. This large a gain strains the assumption of a small change made in the analysis, so the precise value of the gain as calculated is questionable; however, the conclusion that the arrangement of the engine with respect to the airframe can have an important effect on the airplane range remains valid.

Configurations of airplanes that combine all of the effects so far discussed are sketched in figure 16. The numbers on the figure are values taken from the previous calculations for a flight Mach number of 4.0, and engine cycle temperature of 3500° R, a maximum airplane lift-drag ratio of 4, and a center-of-pressure shift on the wing  $c$  of 0.15. The angles and distances are drawn approximately correct. The angles indicated are measured from the flight direction, which is horizontal in the sketches. Configuration 1 (fig. 16(b)) combines all the effects as they have been calculated, including the inlet under the wing. In configuration 2 (fig. 16(c)), the engine inlet is located under the airplane canard surface rather than under the wing. The canard angle of attack is twice the wing angle of attack to yield the static longitudinal stability assumed in appendix H. For the case with the canard fixed at both subsonic and supersonic speeds, it would not be necessary to increase the canard angle of attack for trim at supersonic speeds (see appendix H) with this arrangement.

One of the questions with this arrangement is whether the canard plan area is large enough to "cover" the inlet with its pressure field. Figure 17 presents the ratio of engine-inlet stream-tube area to canard plan area required for the airplane thrust to equal drag and that available for the inlet-canard arrangement sketched at the top of the figure. The pressure field of the canard "covers" the inlet up to the Mach number where the available and required area ratios are equal. For example, for an airplane  $(L/D)_{\max}$  of 4 with  $3500^{\circ}$  R cruise cycle temperature, this arrangement can be used up to  $M = 3.0$ . The curves also show that, for lower airplane lift-drag ratios and lower cycle temperatures, both of which increase the size of the inlet, the Mach number at which the available and required area ratios intersect decreases. These calculations were made for  $c/t$  of 0.10. If the canard moment arm  $t$  is increased, the canard surface becomes smaller and the intersection of the curves of required and available area ratios would shift to a lower Mach number than shown. The interaction of control-surface movements on engine performance and the effect of inlet operating conditions on control forces are undesirable characteristics of this arrangement.

Airplane configuration 3 (fig. 16(d)) in principle also includes all the effects discussed. In this case the inlet under the fuselage nose is substituted for the inlet under the wing. The quantitative advantage of placing the inlet under the nose depends on the drag of the nose. If a radar antenna is required, the airplane nose may be quite blunt, as illustrated, and the drag quite high, and the consequent advantage of locating the inlet there may be appreciable. In figure 16(e) (configuration 4), the inlet is located downstream of a converging half axisymmetric body to take advantage of the reduced Mach number and momentum that theoretically exist in this location.

The results for the second combination, which combines effects of inlet location under wing and jet cant for trim (as illustrated by fig. 11), are presented in figure 18. For an airplane with a maximum  $L/D$  of 4, the range gain is about 12 percent for  $3500^{\circ}$  R cycle temperature at Mach 4.0. These gains are considerably less than those shown in the previous summation.

There are no doubt other configurations that include all the effects thus far considered and certainly many others that include only some of the effects. It is evident that consideration must also be given to the airplane external aerodynamics.

#### Use of Boundary Layer in Engine

This section considers the use of the airframe boundary layer in the engine cycle. Using the airframe boundary layer in the engine cycle may be beneficial to the airplane range for two reasons. A previous section has demonstrated the beneficial effect of engine-inlet momentum reduction due to airframe pressure drag. The airframe friction drag, con-

4077

4077  
CL-2 back

sidered in this section, results in a similar inlet momentum reduction and a consequent possibility of improved range. The second reason that the use of airframe boundary layer may be beneficial to the airplane range is illustrated in figure 19. The propulsive efficiency of an airplane can be measured qualitatively and quantitatively by the velocity disturbance it leaves in the air after having passed through it. Consider, for example, an airplane that has only friction drag and is propelled by a jet engine. The disturbance it leaves in the air is represented by figure 19. The momentum of the friction drag is equal and opposite to the momentum of the engine exhaust jet for the thrust to equal the drag. Considerable energy remains in the air in the form of vorticity. If all the boundary layer is taken into the engine and accelerated back to zero speed (the reference system is fixed in the free stream), the thrust still equals the drag but no disturbance is left in the air. This is clearly a more efficient system. The detailed analysis of a system using airframe boundary layer in the engine cycle is consistent with the previous developments (see appendix K). The results of the analysis are presented in figure 20 for values of  $\eta(C_{D,ofr}/C_{D,o})$  of 0.5 and 1.0.

The term  $\eta(C_{D,ofr}/C_{D,o})$  is the product of two terms, the fraction of the drag at zero lift that is friction, and the fraction of the total boundary-layer-air momentum defect that is captured in the engine. Note from equation (K19) that the fractional change in range is linear with the term  $\eta(C_{D,ofr}/C_{D,o})$ . The limiting value of this parameter is 1.0, which means that all the drag at zero lift is friction drag and that all the boundary layer is taken into the engine. For this limiting case (fig. 20(b)), the change in range is twice that shown in figure 20(a), which was calculated for a value of 0.5.

The more reasonable value of 0.5 may be interpreted as, for example, that about 70 percent of the drag at zero lift is friction and about 70 percent of the boundary-layer momentum defect is captured by the inlet. The total pressure of this air within the engine is assumed to be the product of the pressure recovery of the inlet in the free stream and the total pressure available in the boundary-layer air. The total pressure available in the boundary layer has, of course, been reduced from the free-stream value by friction. For low cycle temperatures, use of boundary layer in the engine shows an advantage above about  $M = 1.2$  for the turbojet and above  $M = 2.0$  for the ram jet; and, for high cycle temperature (i.e.,  $3500^\circ R$ ), above about  $M = 2.8$  for both engines. At  $M = 4.0$  and  $3500^\circ R$  temperature, the gain is about 17 percent in range.

Two possible airplane configurations using airframe boundary-layer air in the engine cycle are shown in figure 21. In configuration A (fig. 21(a)), only the boundary from the underside of the wing is taken into the engine. Above Mach 1.4, at angle of attack the local dynamic pressure and, consequently, the friction forces are considerably larger on the underside of the wing as compared with the upper side. Thus, a large

fraction of the momentum defect due to airframe friction drag may be captured in the engine. Several features of this configuration are also consistent with the previous discussion on airplane arrangement; namely, the engine inlet is under the wing, and the engine exhaust effluxes at the angle of the wing. Still another possible arrangement for a missile is configuration B (fig. 21(b)). This configuration flies on the lift developed by the flat bottom fuselage. A large portion of the airframe boundary-layer air gathers in the pair of vortices that form on the lee side of the body. The engine inlets are located to ingest the boundary layer in these vortices.

It should be appreciated that there are many real problems in trying to handle the nonuniform boundary-layer profiles (frequently referred to as distortion) in the inlet diffuser and through the rest of the engine. This flow distortion may result in poorer pressure recoveries than those assumed - poorer compressor performance in the turbojet and poorer combustion in both ram jet and turbojet.

#### CONCLUSIONS

The following general conclusions can be drawn with regard to the effect of engine-airframe arrangement on airplane range based on the equations derived and calculations made in this report. These effects are related to the engine internal flow. Many important external aerodynamic effects that could be favorable or unfavorable have not been accounted for in the present analysis.

1. For a given maximum engine cycle temperature, the effect on range of engine arrangement is greater for higher flight Mach numbers and for lower airplane lift-drag ratios.

2. The effect on range of inlet location (e.g., under the wing) is approximately independent of engine cycle temperature when account is taken of both inlet momentum reduction and inlet pressure-recovery increase.

3. The effect on range of jet cant to derive lift increases with decreasing engine cycle temperature.

4. The use of moments developed by the engine internal flow can be used to reduce or avoid airplane trim drag.

5. The effects of inlet location, jet cant for lift, and use of engine moments for trim, separately or combined, give significant improvements in airplane range. For example, the combined effects give approximately a 25-percent range increase at a flight Mach number of

4077

4.0 for an engine cruise cycle temperature of  $3500^{\circ}$  R and an airplane with a maximum lift-drag ratio of 4.

6. Use of the airframe boundary layer in the engine cycle shows theoretical gains in airplane range under some conditions; for example, a possible gain of 17 percent at a flight Mach number of 4.0.

Lewis Flight Propulsion Laboratory  
National Advisory Committee for Aeronautics  
Cleveland, Ohio, December 7, 1956

4077

## APPENDIX A

## SYMBOLS

A	cross-sectional area
$A_F$	engine frontal area (compressor frontal area for turbojet, combustor flow area for ram jet)
$A_0$	free-stream-tube area of air entering engine
B $\equiv$	$1 - \frac{C_F}{I} \left( \frac{\partial I}{\partial C_F} \right)_{X, C_D}$
C $\equiv$	$1 - \frac{2C_F}{I} \left( \frac{\partial I}{\partial C_F} \right)_{X, C_D}$
$C_D$	drag coefficient
$C_{D,i}$	drag coefficient due to lift (based on $S_W$ )
$C_{D,o}$	zero-lift drag coefficient of airplane (based on $S_W$ )
$C_F$	engine internal thrust coefficient, $F/qA_F$
$C_L$	wing lift coefficient, $L/qS_W$
$C_{L,opt}$	wing lift coefficient at maximum lift-drag ratio
$\frac{dC_L}{d\alpha}$	airplane lift-curve slope
$C_M$	coefficient of moment = $\frac{\text{Moment about airplane center of gravity}}{q_0 S_W m.a.c.}$
c	wing center-of-pressure shift, fraction of mean aerodynamic chord, positive for a rearward center-of-pressure shift from subsonic to supersonic speeds
D	total airplane drag in steady level flight
$d_D$	moment arm of airplane drag about airplane center of gravity, fraction of mean aerodynamic chord

$d_e$	moment arm of engine-exit momentum about airplane center of gravity, fraction of mean aerodynamic chord
$d_{in}$	moment arm from airplane center of gravity to engine inlet, perpendicular to the free stream at zero angle of attack, fraction of mean aerodynamic chord
$F$	engine internal thrust, $\Phi_e - \Phi_0$ in appendix D and $\Phi_e \cos \theta - \Phi_0$ in appendix G
$F_l$	inlet-location force = $\Phi_0 - \Phi_{in}$ , positive in upstream direction
$f, g$	functions
$I$	engine internal specific impulse, $F/w_f$
$\left(\frac{\partial I}{\partial C_F}\right)_{X, C_D}$	change in engine specific impulse with engine thrust coefficient, where $T_7$ is an intermediate variable (see ref. 2)
$k$	$C_{D,i}/C_L^2$ , equals a constant for a parabolic drag-polar as assumed in this report
$L$	lift
$L/D$	cruise airplane lift-drag ratio
$(L/D)_{max}$	maximum airplane lift-drag ratio
$l_b$	moment arm of airplane lift about airplane center of gravity at subsonic speed, fraction of mean aerodynamic chord
$l_{in}$	moment arm to engine inlet from airplane center of gravity, parallel to the free-stream direction, fraction of mean aerodynamic chord
$l_p$	moment arm of airplane lift about airplane center of gravity at supersonic speed, fraction of mean aerodynamic chord
$M$	Mach number
m.a.c.	mean aerodynamic chord of wing
$N$	force normal to free stream
$P$	total pressure

$P_{in}$	average total pressure at engine air inlet (see fig. 27)
$\frac{P_2}{P_0}$	inlet-diffuser pressure recovery, total pressure at diffuser discharge divided by free-stream total pressure
$p$	static pressure
$q$	free-stream incompressible dynamic pressure, $\frac{\gamma}{2} p_0 M_0^2$
$R$	airplane range
$S$	surface area
$T_7$	engine cycle temperature
$\mathcal{I}$	tail lift force
$t$	tail moment arm about airplane center of gravity, fraction of mean aerodynamic chord
$V$	flight speed
$W$	weight
$W_f$	initial fuel weight
$W_G$	initial airplane gross weight
$w_a$	airflow rate, lb/sec
$w_f$	fuel-flow rate, lb/sec
$X$	parameter being considered
$\alpha$	angle of attack
$\gamma$	ratio of specific heats for ambient air
$\delta$	wing local surface angle
$\eta$	fraction of total boundary-layer-momentum defect that is captured in engine
$\theta$	angle of jet cant, positive downward
$\lambda$	$\alpha + \delta$

~~CONFIDENTIAL~~

$\mu$  Mach angle

$\Phi$  momentum parallel to free-stream direction,

$$\int_A (p - p_0) dA + \int_A \gamma p M^2 dA$$

$\Phi \downarrow$  momentum perpendicular to free-stream direction

Subscripts:

$A_0$  coefficient based on  $A_0$

b subsonic speed

e engine exit

fr friction

in station just ahead of inlet

max maximum

ot zero trim drag

p supersonic speed

T tail

t total

W wing

w station in airplane wake

$\theta$  associated with jet cant

0 station in free stream

0' engine air in free stream

1 airplane prior to modification

2 airplane after modification

Note: Positive directions of distances, forces, moments, and angles are given in fig. 6.

~~CONFIDENTIAL~~

4077

CL-3

## APPENDIX B

## BASIC CONSIDERATION OF THE RANGE EQUATION

The range of an airplane with fixed weight and size is used as a criterion of merit in this report. This appendix develops the basic concepts for use of the range equation for evaluating the modifications considered in this report. The range equation may be written

$$R = V \frac{L}{D} I \ln \left( \frac{1}{1 - \frac{W_F}{W_G}} \right) \quad (B1)$$

For the cases where changes affecting only airplane lift-drag ratio are considered, differentiating logarithmically and assuming a constant  $W_F/W_G$  and  $V$  yield

$$\frac{1}{R} \frac{dR}{dX} = \frac{1}{L/D} \frac{d(L/D)}{dX} + \frac{1}{I} \frac{dI}{dC_F} \frac{dC_F}{dX} \quad (B2)$$

where  $X$  is any parameter being considered such as  $C_D$  or  $P_2/P_0$ .

Reference 2 shows that changes made to an engine (e.g., its drag) installed in an airplane initially flying at maximum  $(L/D)I$  can be evaluated either at constant  $W_G/pS_W$  or at constant engine cycle temperature. For a given airplane,  $W_G$  and  $S_W$  are constant, so that the present evaluations are made at constant airplane altitude where the airplane, before modification, is flying at the altitude for  $[(L/D)I]_{\max}$ .

By equating the thrust to the drag,

$$F = \frac{W_G}{L/D} \quad (B3)$$

by differentiation for a constant gross weight at constant altitude there is obtained

$$\frac{1}{F} \frac{\partial F}{\partial X} = \frac{1}{C_F} \frac{\partial C_F}{\partial X} = - \frac{1}{L/D} \frac{\partial(L/D)}{\partial X} \quad (B4)$$

so that the percent change in range may be written

$$\frac{\Delta R}{R} = \left( \frac{1}{R} \frac{dR}{dX} \right) dX = \left[ 1 - \frac{C_F}{I} \left( \frac{\partial I}{\partial C_F} \right)_{X, C_D} \right] \frac{1}{L/D} \frac{\partial(L/D)}{\partial X} dX \quad (B5)$$

4077

Defining

$$B \equiv 1 - \frac{C_F}{I} \left( \frac{\partial I}{\partial C_F} \right)_{X, C_D} \quad (B6)$$

for convenience in writing,

$$\frac{\Delta R}{R} = B \frac{\Delta(L/D)}{L/D} \quad (B7)$$

The terms defining B are evaluated for a turbojet engine and a ram-jet engine in reference 2, and the term following the bracket in equation (B5) may be evaluated for two configurations being compared:

$$\frac{\Delta(L/D)}{L/D} = \frac{1}{L/D} \left[ \frac{\partial(L/D)}{\partial X} \right] \Delta X = \frac{(L/D)_2 - (L/D)_1}{(L/D)_1} \quad (B8)$$

where the subscripts 1 and 2 refer to the airplane prior to and after modification, respectively. The cases in which the engine thrust is affected by a modification such as jet deflection are dealt with in detail in the appropriate appendix.

## APPENDIX C

DETERMINATION OF CRUISE LIFT COEFFICIENT, ANGLE OF ATTACK, LIFT-DRAG  
RATIO, AND RATIO OF FRICTION DRAG TO TOTAL DRAG

Appendix D of reference 2 gives the following relation between engine and airframe parameters at  $[(L/D)I]_{\max}$ . (A drag polar that is parabolic and symmetrical about  $0^\circ$  angle of attack is assumed in this report and in reference 2. This is an approximation, because the configurations arrived at in this report may be quite unsymmetrical, as shown in fig. 16.)

$$\frac{C_F}{I} \left( \frac{\partial I}{\partial C_F} \right)_{X, C_D} = - \left[ \frac{1 - \left( \frac{C_L}{C_{L, \text{opt}}} \right)^2}{2 \left( \frac{C_L}{C_{L, \text{opt}}} \right)^2} \right] \quad (C1)$$

Equation (C1) may be solved for  $C_L/C_{L, \text{opt}}$  to give

$$\frac{C_L}{C_{L, \text{opt}}} = \left[ \frac{1}{1 - 2 \frac{C_F}{I} \left( \frac{\partial I}{\partial C_F} \right)_{X, C_D}} \right]^{1/2} \quad (C2)$$

Defining

$$C \equiv 1 - 2 \frac{C_F}{I} \left( \frac{\partial I}{\partial C_F} \right)_{X, C_D} \quad (C3)$$

for convenience,

$$\frac{C_L}{C_{L, \text{opt}}} = \frac{1}{C^{1/2}} \quad (C4)$$

The optimum lift coefficient may be determined from

$$C_{L, \text{opt}} = \sqrt{\frac{C_{D, 0}}{k}} \quad (C5)$$

and the maximum lift-drag ratio is then

$$\left(\frac{L}{D}\right)_{\max} = \frac{C_{L,\text{opt}}}{2C_{D,o}} \quad (C6)$$

From equations (C5) and (C6),

$$C_{L,\text{opt}} = \frac{1}{2k(L/D)_{\max}} \quad (C7)$$

Combining equations (C4) and (C7) gives

$$C_L = \frac{1}{2k(L/D)_{\max} C^{1/2}} \quad (C8)$$

This determines the airplane lift coefficient at cruise conditions if the engine operating conditions, the maximum airframe lift-drag ratio, and the drag due to lift coefficient  $k$  are known.

The wing angle of attack is related to the lift coefficient by

$$\alpha_W = \frac{C_L}{\frac{dC_L}{d\alpha}} \quad (C9)$$

For a wing at supersonic speeds with no leading-edge suction,

$$\frac{dC_L}{d\alpha} = \frac{1}{k} \quad (C10)$$

From equations (C8), (C9), and (C10), the wing angle of attack is

$$\alpha_W = \frac{1}{2(L/D)_{\max} C^{1/2}} \quad (C11)$$

The ratio of actual cruise flight  $L/D$  to maximum  $L/D$  may also be found by

$$\frac{L/D}{(L/D)_{\max}} = \frac{C_L}{C_{L,\text{opt}}} \frac{C_{D,o} + kC_{L,\text{opt}}^2}{C_{D,o} + kC_L^2} \quad (C12)$$

For the condition at maximum lift-drag ratio,

$$C_{D,o} = C_{D,i} = kC_{L,opt}^2 \quad (C13)$$

and, using equation (C7),

$$C_{D,o} = \frac{1}{4 \left( \frac{L}{D} \right)_{\max}^2 k} \quad (C14)$$

Equation (C12) reduces to

$$\frac{L/D}{\left( \frac{L}{D} \right)_{\max}} = \frac{C_L}{C_{L,opt}} \frac{2}{1 + \left( \frac{C_L}{C_{L,opt}} \right)^2} \quad (C15)$$

and, using equation (C4),

$$\frac{L/D}{\left( \frac{L}{D} \right)_{\max}} = \frac{2}{C^{1/2} \left( 1 + \frac{1}{C} \right)} \quad (C16)$$

Equation (C2) is plotted in figure 22 for the engine and temperature selected for study in this report. Equation (C16) is plotted in figure 23. For all conditions, except above  $M = 3.4$  at  $2500^\circ R$  engine cycle temperature, the cruise lift coefficient is less than the optimum lift coefficient (fig. 22) and the corresponding cruise lift-drag ratio is less than the maximum lift-drag ratio (fig. 23), as would be expected. Above  $M = 3.4$  at  $2500^\circ R$  cycle temperature, the cruise lift coefficient is greater than the optimum lift coefficient. This occurs because, in equation (C2),  $(\partial I / \partial C_F)$  is positive, meaning that the engine specific impulse would increase if the thrust coefficient or engine cycle temperature were increased (see data of ref. 2). Also, the cruise lift-drag ratio is less than but to the right of the maximum lift-drag ratio. Because of these conditions, the airplane range would increase if the engine cycle temperature were increased, and/or if the cruise lift coefficient were decreased (increased altitudes), which would also require an increase in engine cycle temperature to provide the required increased thrust coefficient. This discussion means that the results calculated and presented in the text above  $M = 3.4$  at  $2500^\circ R$  temperature have practical significance only if for some reason  $2500^\circ R$  is the maximum permissible engine cycle temperature. The same argument applies to conditions above  $M = 4.6$  at  $3500^\circ R$  cycle temperature.

The ratio of friction drag to total airframe drag, in terms of the fraction of drag at zero lift that is friction drag is

$$\frac{D_{fr}}{D_t} = \frac{C_{D,ofr}}{C_{D,t}} = \frac{C_{D,o} \frac{C_{D,ofr}}{C_{D,o}}}{C_{D,o} + kC_L^2} \quad (C17)$$

From the conditions at maximum lift-drag ratio,

$$C_{D,o} = C_{D,i} = kC_{L,opt}^2 \quad (C18)$$

$$C_{D,o} = \frac{1}{4k \left(\frac{L}{D}\right)_{max}^2} \quad (C19)$$

Using equations (C4), (C17), and (C18), the ratio of friction drag to total drag is

$$\frac{D_{fr}}{D_t} = \frac{\frac{C_{D,ofr}}{C_{D,o}}}{1 + \frac{1}{C}} \quad (C20)$$

## APPENDIX D

## EQUATIONS INTERRELATING SEVERAL ENGINE PARAMETERS

This appendix presents relations between several of the engine parameters that occur in this report and those presented in reference 2.

The thrust coefficient of the engine for zero jet cant is defined as

$$F = C_F q A_F = \Phi_e - \Phi_0 \quad (D1)$$

and

$$I = \frac{F}{w_f} \quad (D2)$$

where  $\Phi_0$  is in the free stream. By definition, then,

$$\Phi_0 = 2qA_0 \quad (D3)$$

Thus, a term that appears in appendix G  $\left(\frac{\Phi_e}{w_G} \frac{L}{D}\right)$  becomes

$$\frac{\Phi_e}{w_G} \frac{L}{D} = \frac{\Phi_e}{F} = \left(1 + \frac{2A_0}{C_F A_F}\right) \quad (D4)$$

where the values  $C_F$  and  $A_0/A_F$  are given in reference 2.

The term  $\Phi_{in}/\Phi_e$  that appears in appendix E is hence related to the thrust coefficient by

$$\frac{\Phi_{in}}{\Phi_e} = \frac{1}{1 + \frac{C_F A_F}{2A_0}} \quad (D5)$$

and

$$C_F = \frac{2A_0}{A_F} \left( \frac{1}{\frac{\Phi_{in}}{\Phi_e}} - 1 \right) \quad (D6)$$

The term  $\Phi_e/W_G$  in appendix H may be found from

$$\frac{\Phi_e}{W_G} = \left( \frac{\Phi_e}{W_G} \frac{L}{D} \right) \frac{(L/D)_{\max}}{L/D} \frac{1}{(L/D)_{\max}} \quad (D7)$$

and, using equation (D4) and equation (C16),

$$\frac{\Phi_e}{W_G} = \left( 1 + \frac{2A_O}{C_F A_F} \right) \frac{C^{1/2} (1 + C)}{2} \frac{1}{(L/D)_{\max}} \equiv H \quad (D8)$$

Also,  $\Phi_e/W_G$  may be written

$$\frac{\Phi_e}{W_G} = \frac{1}{\frac{L}{D} \left( 1 - \frac{\Phi_{in}}{\Phi_e} \right)} \quad (D9)$$

Similarly, the term  $\Phi_{in}/W_G$  is

$$\frac{\Phi_{in}}{W_G} = \frac{1}{L/D} \frac{1}{\left( \frac{1}{\frac{\Phi_{in}}{\Phi_e}} - 1 \right)} \quad (D10)$$

Also, the following relation results from equating the engine thrust to the airplane drag:

$$C_F q A_F = F = D = \frac{C_L q S_W}{L/D} \quad (D11)$$

from which

$$\frac{A_O}{S_W} = \frac{A_O}{A_F} \frac{C_L}{C_F} \frac{1}{L/D} = \frac{A_O}{A_F} \frac{1}{C_F} \frac{1 + \frac{1}{C}}{4k(L/D)_{\max}^2} \quad (D12)$$

where it is assumed that  $k$  has the two-dimensional value

$$k = \frac{\sqrt{M^2 - 1}}{4}$$

A numerical value for  $k$  is required only in the discussion of the ratio of engine-inlet area to canard plan area. In this application,  $M$  is greater than 2.0.

## APPENDIX E

## EFFECT ON RANGE OF ENGINE-INLET MOMENTUM REDUCTION

## DUE TO AIRFRAME PRESSURE DRAG

The use of inlet locations that reduce the inlet momentum to the engine to achieve an improvement in airplane range is discussed herein. It is assumed that the inlet total-pressure recovery is not affected. The effect of pressure-recovery change is discussed in appendix F. Using the nomenclature of figure 24, the conventional definition of drag applied to the airframe is

$$-D = \Phi_w + \Phi_{in} - \Phi_0 - \Phi_0' \quad (E1)$$

where the momentum  $\Phi$  is defined as

$$\Phi = \int_A (p - p_0) dA + \int_A \rho p M^2 dA$$

and integration over  $A$  is perpendicular to the free stream. The corresponding engine thrust must then be

$$F = \Phi_e - \Phi_{in} \quad (E2)$$

But the conventional definition of thrust is

$$F' = \Phi_e - \Phi_0' \quad (E3)$$

and this definition will be maintained in this analysis. The drag corresponding to the conventional thrust definition must then be

$$-D = \Phi_w - \Phi_0' \quad (E4)$$

which may be written

$$-D = \left[ \Phi_w + \Phi_{in} - \Phi_0 - \Phi_0' \right] - (\Phi_{in} - \Phi_0') \quad (E5)$$

so that the relation of the new drag definition (eq. (E4)) to the conventional definition (the term in brackets in eq. (E5)) is clear. The term by which the conventional drag definition must be modified as an inlet location force is defined

$$-F_L = \Phi_{in} - \Phi_0' \quad (E6)$$

and, in coefficient form,

$$-C_{F_L, A_0} = \frac{\Phi_{in} - \Phi_{O'}}{\frac{\gamma}{2} \rho_0 M^2 A_0} \quad (E7)$$

or, based on wing area,

$$C_{F_L} = C_{F_L, A_0} \frac{A_0}{S_W} \quad (E8)$$

The term  $C_{F_L}$  may now be treated as part of the airframe drag; for example,

$$\frac{L}{D} = \frac{C_L}{C_D} = \frac{C_L}{C_{D,0} - C_{F_L} + kC_L^2} \quad (E9)$$

and, of course, will be advantageous to the  $L/D$  if it is positive.

If there is a drag on the airframe,  $\Phi_{in}$  will be less than  $\Phi_{O'}$ , yielding a positive drag by the definition

$$-D_L = \Phi_{in} - \Phi_{O'} \quad (E10)$$

But

$$-F_L = \Phi_{in} - \Phi_{O'} \quad (E11)$$

so that

$$-F_L = -D_L \quad (E12)$$

or

$$C_{F_L} = C_{D_L, A_0} \frac{A_0}{S_W} \quad (E13)$$

This says that, in general, if the engine air inlet is located in the vicinity of the fuselage or wing that has drag, the inlet can be expected to feel a reduced inlet momentum compared with the free-stream value. This may be interpreted as an effective reduction in wing or fuselage drag, as is done in this part of the analysis, or as an increase in engine thrust.

Further consideration will be given to the case where the inlet is under the wing. From figure 25, the following relations may be written for small deflection angles, assuming no leading-edge suction, and not accounting for a fuselage upwash:

$$N = \Phi_0 (\alpha_W + \delta) = 2qA_0 (\alpha_W + \delta) \quad (E14)$$

$$D = N(\alpha_W + \delta) = 2qA_0 (\alpha_W + \delta)^2 \quad (E15)$$

$$C_{D,A_0} = 2(\alpha_W + \delta)^2 \quad (E16)$$

From the development in appendix C relating the wing angle of attack to engine operating conditions and airplane  $L/D$ ,

$$\alpha_W = \frac{1}{2(L/D)_{\max} C^{1/2}} \quad (E17)$$

Considering the previous discussion to relate to the local wing condition, the over-all airplane characteristics remain characterized by

$$\alpha_W = \frac{C_L}{\frac{dC_L}{d\alpha}} \quad (E18)$$

and

$$k = \frac{1}{\frac{dC_L}{d\alpha}} \quad (E19)$$

Combining equations (B7), (B8), (E13), (E16), and (E17), and assuming a double-wedge airfoil,

$$\frac{\Delta R}{R} = \frac{B}{C_F A_F} \left[ \frac{1}{2(L/D)_{\max} C^{1/2}} + \tau \right]^2 - 1 \quad (E20)$$

where  $\tau$  is the thickness-to-chord ratio of the wing. This development has assumed no change in inlet total-pressure recovery (total pressure at compressor face, or combustor divided by free-stream total pressure) with a change in inlet momentum. The effect of inlet pressure recovery is discussed in appendix F.

It has also been assumed that the configuration lift has not been affected by locating the inlet under the wing. There are two points of view that may be taken here. The simplest is illustrated in figure 2. The wing lift on the surface a, generated by deflecting air downward, is lost if the air is captured by the inlet and exhausted in the free-stream direction. It may be assumed that the lift on the engine surface a' makes up for the wing lift lost from the surface a. The same argument may then be applied to the surfaces b and b'. The surfaces a and b are only a fraction of the total wing area. In this point of view, the total airplane lift is conserved by considering the lift of the external flow over the engine; the engine exhaust jet is in the free-stream direction; and equation (E20) applies.

The second point of view that can be taken to conserve the total lift of the configuration is to conserve the downward momentum of air by canting the exhaust jet slightly downward. The direction of the flow under the wing associated with the lift is  $\alpha_W$ , and the downward momentum of the air handled by the engine would be

$$\Phi_{\downarrow in} = \Phi_0'(\alpha) \quad (E21)$$

(There is also a flow deflection associated with the wing thickness and drag that is not considered here.) To keep the same downward momentum at the exit of the engine,

$$\Phi_{\downarrow e} = \Phi_e \theta \quad (E22)$$

From these relations and equation (D5),

$$\theta \Phi_{\downarrow in} = \frac{\Phi_0'}{\Phi_e} (\alpha_W) = \left( \frac{1}{1 + \frac{C_{FAF}}{2A_0}} \right) \alpha_W \quad (E23)$$

where  $\theta \Phi_{\downarrow in}$  is the jet cant required to avoid changing the wing and/or total lift as calculated without the presence of the engine. The thrust of the engine has now been decreased because the exhaust jet is no longer in the free-stream direction. The decrease in thrust is for small angles

$$F_\theta - F = - \Phi_e (1 - \cos \theta) = - \Phi_e \theta^2 \Phi_{\downarrow in} \quad (E24)$$

Using this relation and equations (E23) and (D4), equation (E20) becomes

$$\frac{\Delta R}{R} = \frac{B}{C_{FAF}} \frac{1}{2A_0 \left\{ \left[ \frac{1}{2(L/D)_{\max} C^{1/2}} + \tau \right]^2 - \left[ \frac{1}{1 + \frac{C_{FAF}}{2A_0}} \right] \left[ \frac{1}{2(L/D)_{\max} C^{1/2}} \right]^2 \right\}} \quad (E25)$$

Equation (E25) will yield range increases less than equation (E20). For example, at  $M = 4.0$ ,  $(L/D)_{\max} = 4.0$ , and a cycle temperature of  $3500^\circ R$ , equation (E20) gives  $\Delta R/R = 0.0577$ , while equation (E25) gives  $\Delta R/R = 0.0356$ . Equation (E20) is evaluated in figure 3.

~~CONFIDENTIAL~~

## APPENDIX F

## EFFECT ON RANGE OF AN INCREASE IN PRESSURE

## RECOVERY DUE TO INLET LOCATION

In addition to the increase in range that results because of the reduced inlet momentum when an inlet is located under a wing, there is also an increase in range because of an increase in inlet pressure recovery. The pressure recovery is defined as the total pressure at the diffuser discharge divided by free-stream total pressure. This development assumes the inlet momentum is that in the free stream. The results of the pressure-recovery increase (this appendix) and the effect of inlet momentum reduction (appendix E) are thus additive. According to reference 2 (p. 25), the change in range with pressure recovery is

$$\frac{\Delta R}{R} = \frac{1}{I} \left[ \frac{\partial I}{\partial \left( \frac{P_2}{P_0} \right)} - \left( \frac{\partial I}{\partial C_F} \right)_{X, C_D} \frac{\partial C_F}{\partial \left( \frac{P_2}{P_0} \right)} \right] \Delta \left( \frac{P_2}{P_0} \right) \quad (F1)$$

where the subscript X is  $P_2/P_0$ . The change in pressure recovery  $\Delta(P_2/P_0)$  may be evaluated if the wing angle of attack (from appendix C), wing thickness, and the inlet pressure-recovery Mach number characteristics are known.

Figure 26 gives the relation of pressure recovery ( $P_2/P_0$  or  $P_2/P_{in}$ ) and Mach number for the inlet assumed in this report. The inlet has the pressure recovery through two oblique shocks and one normal shock and a subsonic recovery of 0.95. Knowing the wing angle of attack and thickness, the local Mach number and local total pressure may be found from charts available, for example, in reference 3. In this case, for example, the inlet which is normally a three-shock inlet (two oblique and one normal) becomes effectively a four-shock inlet by placing it under the wing. Pressure recovery consequently improves.

~~CONFIDENTIAL~~

## APPENDIX G

## EFFECT ON RANGE OF EXHAUST-JET CANT FOR LIFT

This appendix deals with the use of jet cant to obtain lift. The point of view is again taken that an airplane of fixed-size components such as wing, engine, and fuselage, is given, and it is desired to find the change in range due to canting the exhaust jet downward. The inlet of the engine is assumed to be in the free stream. It is convenient in this case to write the range equation as

$$R = V \frac{W_G}{W_F} \ln \frac{1}{1 - \frac{W_F}{W_G}} \quad (G1)$$

so that, by logarithmic differentiation with respect to jet deflection  $\theta$ , the percent change in range may be written for a constant fuel-to-gross-weight ratio:

$$\frac{\Delta R}{R} = - \frac{1}{W_F} \int_0^\theta \frac{dw_F}{d\theta} d\theta \quad (G2)$$

Again, this change may be evaluated at constant ambient flight pressure, assuming the airplane is initially flying at conditions of minimum fuel flow  $[(L/D)I]_{\max}$  for no jet deflection. Also, of course, the minimum fuel-flow rate will occur for the jet deflection  $\theta$  where  $dw_F/d\theta = 0$ . Equating the forces in the lift direction gives

$$W_G = L_W + L_\theta \quad (G3)$$

The definitions of thrust and specific impulse used in appendix D are

$$F = \Phi_e - \Phi_0 \quad (G4)$$

and

$$I = \frac{F}{W_F} \quad (G5)$$

Because the jet cant  $\theta$  is now to be a variable, consider a new definition for thrust and specific impulse; at a given cycle temperature,

$$F' = \Phi_e \cos \theta - \Phi_0 \quad (G6)$$

and

$$I' = \frac{F'}{w_f} \quad (G7)$$

or,

$$F' = F \left( \frac{F'}{F} \right) \quad (G8)$$

and

$$I' = I \left( \frac{F'}{F} \right) \quad (G9)$$

In equation (G2) the quantity of interest is the fuel-flow rate. From equations (G4) and (G5), the fuel-flow rate is

$$w_f = \frac{F}{I} \quad (G10)$$

From equations (G8) and (G9), the fuel-flow rate is

$$w_f = \frac{F'}{I'} = \frac{F \left( \frac{F'}{F} \right)}{I \left( \frac{F'}{F} \right)} = \frac{F}{I} \quad (G11)$$

Hence, comparison of equations (G10) and (G11) shows that the fuel-flow rate is independent of the definition of thrust and specific impulse. The definitions given by (G6) and (G7) will be used in this section, but the primes will not be shown.

From equation (G11), by differentiation,

$$\frac{1}{w_f} \frac{dw_f}{d\theta} = - \frac{1}{I} \frac{dI}{d\theta} + \frac{1}{C_F} \frac{dC_F}{d\theta} \quad (G12)$$

where  $dI/d\theta$  is to be evaluated for the thrust equal to the drag; and, for the thrust equal to the drag,

$$\frac{1}{C_F} \frac{dC_F}{d\theta} = \frac{1}{C_D} \frac{dC_D}{d\theta} \quad (G13)$$

so equation (G12) may be written

$$\frac{1}{w_f} \frac{dw_f}{d\theta} = - \frac{1}{I} \frac{dI}{d\theta} + \frac{1}{C_D} \frac{dC_D}{d\theta} \quad (G14)$$

In subsequent portions of the development, changes will be evaluated from the condition of zero jet deflection.

Evaluating first the term in equation (G14) involving the airplane drag,

$$C_D = C_{D,o} + kC_L^2 \quad (G15)$$

and differentiating,

$$\frac{dC_D}{d\theta} = 2kC_L \frac{dC_L}{d\theta} \quad (G16)$$

But

$$C_L = \frac{W_G - L_\theta}{qS_W} \quad (G17)$$

so that

$$\frac{dC_L}{d\theta} = - \frac{1}{qS_W} \frac{dL_\theta}{d\theta} \quad (G18)$$

and, substituting in equation (G16) and making a fraction of the drag at zero jet deflection,

$$\frac{1}{C_D} \frac{dC_D}{d\theta} = - \frac{L/D}{W_G} 2kC_L \frac{dL_\theta}{d\theta} \quad (G19)$$

From figure 6, the lift due to jet deflection is

$$L_\theta = \Phi_e \sin \theta \quad (G20)$$

and

$$\frac{dL_\theta}{d\theta} = \Phi_e \cos \theta + d\Phi_e \sin \theta \quad (G21)$$

where the last term is neglected compared with the first term on the right side of the equation assuming relatively small  $\theta$ , and equation (G19) becomes

$$\frac{1}{C_D} \frac{dC_D}{d\theta} = - \frac{L}{D} 2kC_L \frac{\Phi_e}{W_G} \cos \theta \quad (G22)$$

This is also the change in the required engine thrust coefficient, as previously pointed out in equation (G13):

$$\frac{1}{C_F} \left( \frac{dC_F}{d\theta} \right) = \frac{1}{C_D} \frac{dC_D}{d\theta} \quad (G23)$$

The term in equation (G14) involving the specific impulse may now be evaluated. The engine thrust coefficient and specific impulse are a function of the following variables:

$$I = f_1(\theta, T_7); \quad T_7 = g_1(\theta) \quad (G24)$$

$$C_F = f_2(\theta, T_7); \quad T_7 = g_2(\theta) \quad (G25)$$

so that, by differentiation,

$$\frac{dI}{d\theta} = \left( \frac{\partial I}{\partial \theta} \right)_{T_7} + \frac{\partial I}{\partial C_F} \left( \frac{dC_F}{dT_7} \frac{dT_7}{d\theta} \right) \quad (G26)$$

$$\frac{dC_F}{d\theta} = \left( \frac{\partial C_F}{\partial \theta} \right)_{T_7} + \left( \frac{\partial C_F}{\partial T_7} \frac{dT_7}{d\theta} \right) \quad (G27)$$

Combining equations (G26) and (G27) gives

$$\frac{1}{I} \frac{dI}{d\theta} = \frac{1}{I} \left( \frac{\partial I}{\partial \theta} \right)_{T_7} + \left( \frac{\partial I}{\partial C_F} \right) \frac{C_F}{I} \left[ \frac{1}{C_F} \left( \frac{dC_F}{d\theta} \right) - \frac{1}{C_F} \left( \frac{\partial C_F}{\partial \theta} \right)_{T_7} \right] \quad (G28)$$

From equation (G6) for engine thrust,

$$F = \Phi_e \cos \theta - \Phi_0 \quad (G29)$$

$$\frac{1}{C_F} \left( \frac{dC_F}{d\theta} \right)_{T_7} = - \frac{L}{D} \frac{\Phi_e}{W_G} \sin \theta \quad (G30)$$

as a fraction of the thrust coefficient for zero jet deflection. Similarly, for the specific impulse,

$$\frac{1}{I} \left( \frac{\partial I}{\partial \theta} \right)_{T_7} = \frac{1}{C_F} \left( \frac{dC_F}{d\theta} \right)_{T_7} = - \frac{L}{D} \frac{\Phi_e}{W_G} \sin \theta \quad (G31)$$

Substituting equations (G22), (G23), (G29), and (G31) in (G28) gives

$$\frac{1}{I} \frac{dI}{d\theta} = \frac{\phi_e}{W_G} \frac{L}{D} \left[ -\sin \theta + \frac{C_F}{I} \left( \frac{\partial I}{\partial C_F} \right) (-2kC_L \cos \theta + \sin \theta) \right] \quad (G32)$$

Equations (G22), (G32), (B6), and (D4) may be combined with equation (G14) to yield

$$\frac{1}{w_F} \frac{dw_F}{d\theta} = - \left( 1 + \frac{2A_O}{C_F A_F} \right) B (2kC_L \cos \theta - \sin \theta) \quad (G33)$$

(The term B involving the engine performance and derivatives is the same previously encountered in the general discussion of the range equations, appendix B.) The deflection angle for maximum increase in range is found by setting equation (G33) equal to zero and using the result in appendix C for  $C_L$ :

$$\tan \theta = 2kC_L = \frac{1}{(L/D)_{\max} C^{1/2}} \quad (G34)$$

Note that, from a comparison of equations (G34) and (C11), the optimum angle of jet cant is approximately twice the wing angle of attack.

Equation (G33) may be integrated directly to get the percent changes in fuel flow for any deflection angle:

$$\left( \frac{\Delta R}{R} \right)_{\theta} = - \frac{\Delta w_F}{w_F} = \left( 1 + \frac{2A_O}{C_F A_F} \right) B \left[ \frac{1}{(L/D)_{\max} C^{1/2}} \sin \theta + \cos \theta - 1 \right] \quad (G35)$$

A simplified form of the results given by equation (G34) and (G35) may be derived for small angles and optimum cant. Thus,

$$\theta \cong \sin \theta \cong \tan \theta \cong \frac{1}{(L/D)_{\max} C^{1/2}} \quad (G36)$$

Assuming a parabolic variation of  $\Delta R/R$  with  $\theta$  from zero to optimum angle of cant with the vertex of the parabola at the optimum angle, the average rate of change is half the initial value. Thus, evaluating (G35) at  $\theta = 0$  and taking  $d\theta = \theta$  yield

$$\frac{\Delta R}{R} = \frac{1}{2} \left( 1 + \frac{2A_O}{C_F A_F} \right) \frac{B}{(L/D)_{\max}^2 C} \quad (G37)$$

~~CONFIDENTIAL~~

If the airplane is flying at  $(L/D)_{\max}$ , so that  $(\partial I / \partial C_F) = 0$ , then equations (G34) and (G35) become

$$\tan \theta = \frac{1}{(L/D)_{\max}} \quad (G38)$$

and

$$\frac{\Delta R}{R} = \left( 1 + \frac{2A_0}{C_F A_F} \right) \left[ \frac{1}{(L/D)_{\max}} \sin \theta + \cos \theta - 1 \right] \quad (G39)$$

For both small angles and the airplane flying at  $(L/D)_{\max}$ ,

$$\theta \approx \sin \theta \approx \tan \theta \approx \frac{1}{(L/D)_{\max}} \quad (G40)$$

and

$$\frac{\Delta R}{R} = \frac{1}{2} \left( 1 + \frac{2A_0}{C_F A_F} \right) \frac{1}{(L/D)_{\max}^2} \quad (G41)$$

[Note that, in comparing the symbols of this appendix with those of reference 2,  $(\partial I / \partial C_F) = (\partial I / \partial C_F)_{X, C_D}$ .]

The cases just calculated are for the inlet in the free stream. For the inlet under the wing, an interpretation of the present result is required. The angle of jet cant that is equivalent to deriving no lift from the jet is given by equation (E23). Thus, the gain as calculated in this section from zero jet cant to the angle for zero lift (appendix E) is in reality nonexistent. The correct gain is the difference between the gain at any given jet deflection and the gain shown for the jet deflection for no change in downward momentum with the inlet under the wing.

~~CONFIDENTIAL~~

## APPENDIX H

## EFFECT ON RANGE OF TRIM DRAG

This appendix considers the effect of trim drag on the range of airplanes with three trimming arrangements: the conventional fixed tail, a fixed canard, and a floating or fixed canard.

## Conventional Fixed Tail

On the assumption that the engine airflow moments are used to counteract the moment due to wing center-of-pressure shift, the gain in range resulting from the elimination of the trim drag at supersonic speeds may be estimated. Figure 10 illustrates the symbols used. The airplane has a tail to the rear and neutral tail-off longitudinal static stability at subsonic speeds.

The airplane longitudinal static stability with tail on at subsonic speeds is then described by the contribution of the tail to the stability:

$$\frac{dC_M}{d\alpha} = - \frac{S_{Tt}}{S_W} \left( \frac{dC_L}{d\alpha} \right)_T \quad (H1)$$

The airplane weight-to-drag ratio (weight is defined as positive upward only on the left side of the equations for airplane weight-to-drag ratio) for no trim at supersonic speeds is

$$\left( \frac{W}{D} \right)_{ot} = \frac{C_{L,W,ot}}{C_{D,o} + kC_{L,W,ot}^2} \quad (H2)$$

where

$$C_{L,W,ot} = \frac{W}{qS_W} \quad (H3)$$

This W/D can be compared with the W/D ratio of an airplane that required a tail to trim out the effect of wing center-of-pressure shift from subsonic to supersonic speed. The comparison is made at the same flight altitude for the two cases. Summing the moments and forces about the airplane center of gravity at supersonic speeds gives

$$\Sigma(\text{moments}) = - cL_p - t\mathcal{F} = 0 \quad (H4)$$

$$\Sigma(\text{forces}) = L_p + \mathcal{F} - W = 0 \quad (H5)$$

From the relations (H3), (H4), and (H5),

$$C_{L,W} = \frac{C_{L,W,ot}}{1 - \frac{c}{t}} \quad (H6)$$

and

$$C_{L,T} = - C_{L,W} \frac{c}{t} \frac{S_W}{S_T} \quad (H7)$$

If it is assumed the tail is designed so that  $C_{L,T} = - C_{L,W}$ , then

$$\frac{c}{t} \frac{S_W}{S_T} = 1.0 \quad (H8)$$

and, assuming the same drag due to lift coefficient  $k$  for the wing and tail, the airplane weight-drag ratio is

$$\left(\frac{W}{D}\right)_t = \frac{C_{L,W} \left(1 - \frac{c}{t}\right)}{C_{D,o} + k \left(1 + \frac{c}{t}\right) C_{L,W}^2} \quad (H9)$$

In terms of the lift coefficient on the wing for no trim drag,

$$\left(\frac{W}{D}\right)_t = \frac{C_{L,W,ot}}{C_{D,o} + \frac{k \left(1 + \frac{c}{t}\right)}{\left(1 - \frac{c}{t}\right)^2} C_{L,W,ot}^2} \quad (H10)$$

The fractional change in weight-to-drag ratio or lift-drag ratio in terms of the airplane  $L/D$  with zero trim drag is, by equation (B8),

$$\frac{\Delta \left(\frac{L}{D}\right)}{\frac{L}{D}} = \frac{\left(\frac{W}{D}\right)_t - \left(\frac{W}{D}\right)_{ot}}{\left(\frac{W}{D}\right)_{ot}} = \frac{C_{D,o} + k C_{L,W,ot}^2}{C_{D,o} + k C_{L,W,ot}^2 \frac{\left(1 + \frac{c}{t}\right)}{\left(1 - \frac{c}{t}\right)^2}} - 1 \quad (H11)$$

4011

and, from equations (C8), (C14), and (B7),

$$\frac{\Delta R}{R} = B \left[ \frac{1 + \frac{1}{C}}{1 + \frac{1 + \frac{c}{t}}{C \left(1 - \frac{c}{t}\right)^2}} - 1 \right] \quad (\text{H12})$$

As a special case, if the airplane was flying at maximum lift-drag ratio for the case of no trim drag,

$$C_{D,o} = k C_{L,opt,W,ot}^2 \quad (\text{H13})$$

and equation (H11) becomes

$$\frac{\Delta \left( \frac{L}{D} \right)}{\frac{L}{D}} = \frac{2}{1 + 1 \frac{\left(1 + \frac{c}{t}\right)^2}{\left(1 - \frac{c}{t}\right)^2}} - 1 \quad (\text{H14})$$

#### Fixed Canard

For the "fixed-canard" case, the trimming surface is ahead of the wing and, for stability calculations, the canard surface is fixed with respect to the fuselage at both subsonic and supersonic speeds. The canard arrangement is defined to have the same longitudinal static stability, same wing area, same canard area, same moment arm, and same lift-curve slope as the airplane of conventional tail arrangement.

The sum of the forces and moments at subsonic speed gives

$$\Sigma (\text{moments}) = - L_b L_b - t \mathcal{F} = 0 \quad (\text{H15})$$

$$\Sigma (\text{forces}) = L_b + \mathcal{F} - W = 0$$

where

$$\mathcal{F} = C_{L,T} S_T \quad (\text{H16})$$

$$L_b = C_{L,W} S W$$

Now,

$$\frac{dC_M}{d\alpha} = - \left( \frac{dC_L}{d\alpha} \right)_W l_b + \left( \frac{dC_L}{d\alpha} \right)_T \frac{S_T}{S_W} t \quad (H17)$$

and, if equation (H1) is used to get the same static stability, equation (H17) becomes

$$- \frac{S_T}{S_W} t \left( \frac{dC_L}{d\alpha} \right)_T = - \left( \frac{dC_L}{d\alpha} \right)_W l_b + \left( \frac{dC_L}{d\alpha} \right)_T \frac{S_T}{S_W} t \quad (H18)$$

By equation (H8) in the discussion of the conventional arrangement, and accounting for the difference in sign of  $t$  and  $c$ ,

$$\frac{c}{t} \frac{S_W}{S_T} = - 1.0 \quad (H19)$$

and, assuming the same lift-curve slope for wing and tail and using (H19),

$$l_b = 2t \frac{S_T}{S_W} = - 2c \quad (H20)$$

Then, by equations (H15), (H16), (H19), and (H20),

$$C_{L,T} = 2C_{L,W} \quad (H21)$$

or  $\alpha_T = 2\alpha_W$  at subsonic speeds. At supersonic speeds, then,

$$\Sigma(\text{forces}) = 0 = L_p + \mathcal{J} - W$$

$$\Sigma(\text{moments}) = 0 = - l_p L_p - t\mathcal{J} = - 3cL_p - t\mathcal{J} \quad (H22)$$

or

$$C_{L,W} + C_{L,T} \frac{S_T}{S_W} - \frac{W_G}{qS_W} = 0 \quad (H23)$$

$$3cC_{L,W} + tC_{L,T} \frac{S_T}{S_W} = 0$$

from which, at supersonic speeds,

$$C_{L,T} = 3C_{L,W}$$

$$\alpha_T = 3\alpha_W$$

and

$$C_{L,W} \left( 1 + 3 \frac{S_T}{S_W} \right) = \frac{W_G}{qS_W} = C_{L,W,ot} \quad (H24)$$

The weight-to-drag ratio of the trimmed airplane is

$$\left( \frac{W}{D} \right)_t = \frac{C_{L,W} \left( 1 + 3 \frac{c}{t} \right)}{C_{D,o} + k \left( 1 + 3 \frac{c}{t} \right) C_{L,W}^2} \quad (H25)$$

or, in terms of the wing lift coefficient with no airplane trim drag,

$$\left( \frac{W}{D} \right)_t = \frac{C_{L,W,ot}}{C_{D,o} + k \frac{C_{L,W,ot}^2}{\left( 1 + 3 \frac{c}{t} \right)}} \quad (H26)$$

By equation (B8),

$$\frac{\Delta \left( \frac{L}{D} \right)}{\frac{L}{D}} = \frac{\left( \frac{W}{D} \right)_t - \left( \frac{W}{D} \right)_{ot}}{\left( \frac{W}{D} \right)_{ot}} = \frac{C_{D,o} + k C_{L,W,ot}^2}{C_{D,o} + k \frac{C_{L,W,ot}^2}{\left( 1 + 3 \frac{c}{t} \right)}} - 1 \quad (H27)$$

and from equations (C8), (C14), and (B7),

$$\frac{\Delta R}{R} = B \left[ \frac{1 + \frac{1}{C}}{1 + \frac{1}{C \left( 1 + 3 \frac{c}{t} \right)}} - 1 \right] \quad (H28)$$

#### Fixed-Floating Canard

In the fixed-floating canard case, the canard surface is free floating at subsonic speeds but fixed with respect to the fuselage at supersonic speeds. A free-floating canard does not contribute to the stability, although it may produce a force or moment. The angle of attack, and hence the lift, of a free-floating canard is determined by a controllable trim tab on the canard surface. The lift of the free-floating canard

must be independent of changes of angle of the fuselage to which it is attached. Equation (H1) expressing the airplane longitudinal static stability at subsonic speeds thus becomes, because the canard has no destabilizing effect,

$$\frac{dC_M}{d\alpha} = - \frac{dC_L}{d\alpha} l_b \quad (H29)$$

and the final equation giving the percent change in range due to trim drag becomes

$$\frac{\Delta R}{R} = B \left[ \frac{1 + \frac{1}{C}}{1 + \frac{1}{C \left(1 + 2 \frac{c}{t}\right)}} - 1 \right] \quad (H30)$$

## APPENDIX I

## JET CANT FOR AIRPLANE TRIM

This appendix considers the case where the engine exhaust is located at the rear of the airplane and has the same moment arm as the horizontal tail, as illustrated in figure 11. The down load required at the rear of the airplane for trim (discussed in appendix H), may now be supplied by deflecting the jet upward. This, of course, is inconsistent with obtaining lift from the jet as discussed in appendix G; however, it is of interest to compare the technique for trimming the airplane with that of using the tail. The following development compares an airplane with a center-of-gravity location such that the trim drag is zero with an airplane trimmed by deflecting the jet upward. Both airplanes are at the same altitude, the first airplane being at the altitude for maximum  $(L/D)_I$ .

The force  $\mathcal{F}$  supplied by the conventional tail for that case in appendix H is now supplied by the jet, so that

$$\mathcal{F} = \Phi_e \sin \theta \quad (I1)$$

and, from the moments on the airplane,

$$\mathcal{F} = - \frac{c}{t} \frac{W_G}{1 - \frac{c}{t}} \quad (I2)$$

from which

$$\sin \theta = \frac{- \frac{c}{t}}{\frac{\Phi_e}{W_G} \left(1 - \frac{c}{t}\right)} = \frac{- \frac{c}{t}}{H \left(1 - \frac{c}{t}\right)} \quad (I3)$$

where  $\theta$  is defined as positive for downward cant. Equation (I3) may be substituted in equation (G35), which was originally derived to consider the lift jet, to yield

$$\frac{\Delta R}{R} = \left(1 + \frac{2A_O}{C_{FAF}}\right) B \left[ \frac{1}{\left(\frac{L}{D}\right)_{\max} c^{1/2}} \frac{- \frac{c}{t}}{H \left(1 - \frac{c}{t}\right)} + \cos \arcsin \frac{- \frac{c}{t}}{H \left(1 - \frac{c}{t}\right)} - 1 \right] \quad (I4)$$

where  $H$  is defined by equation (D8).

4077  
CI-5 back

APPENDIX J

MOMENTS DEVELOPED BY ENGINE INTERNAL FLOW FOR TRIM

This appendix discusses in a more general way than appendix I the moments than can be developed by the internal engine flow to counteract the center-of-pressure shift on the wing in going from subsonic to supersonic speeds. This discussion is applicable to the cruise conditions at subsonic and supersonic speeds rather than to conditions of accelerations. The basic idea is that, as the airplane center of lift shifts rearward in going from subsonic to supersonic speeds, the drag and thrust also increase. Also, the change in inlet momentum as a fraction of exit momentum may be used. Because the center-of-pressure and engine thrust changes are concomitant, their moments can be arranged to counteract each other. Figure 13 illustrates in the form of special cases the forces and moment arms that are considered in this analysis. The equations developed hold for small angles of attack and are sufficiently detailed for the present purpose.

The sum of the moments (tail off) about the center of gravity is, for subsonic and supersonic speeds, respectively,

$$\Sigma(\text{moments})_b = D_b d_D - L_b l_b + \Phi_{in,b}(d_{in} - l_{in} \sin \alpha_b) - \Phi_{e,b} d_e \quad (J1)$$

$$\Sigma(\text{moments})_p = D_p d_D - L_p l_p + \Phi_{in,p}(d_{in} - l_{in} \sin \alpha_p) - \Phi_{e,p} d_e \quad (J2)$$

To eliminate the trim drag, it is desired that these moments be equal to zero at both flight speeds. Setting equations (J1) and (J2) equal to zero and subtracting and using the relations

$$L = W \quad (J3)$$

and

$$D = F = \Phi_e - \Phi_{in} \quad (J4)$$

give

$$\frac{d_D}{c} \left[ \frac{1}{(L/D)_p} - \frac{1}{(L/D)_b} \right] - 1 + \frac{d_{in}}{c} \left[ \left( \frac{\Phi_{in}}{W_G} \right)_p - \left( \frac{\Phi_{in}}{W_G} \right)_b \right] - \frac{l_{in}}{c} \left[ \left( \frac{\Phi_{in} \sin \alpha}{W_G} \right)_p - \left( \frac{\Phi_{in} \sin \alpha}{W_G} \right)_b \right] - \frac{d_e}{c} \left[ \left( \frac{\Phi_e}{W_G} \right)_p - \left( \frac{\Phi_e}{W_G} \right)_b \right] = 0 \quad (J5)$$

The application of equation (J5) is most easily understood by considering three special cases.

#### Case I

For case I, the following assumptions are made: The axis of the engine is straight and aligned with the flight direction;  $d_D = 0$ ;  $d_{in} - l_{in} \sin \alpha = d_e$ ; and  $\alpha_b = \alpha_p$  or  $l_{in} = 0$ . The airplane angle of attack may well be nearly the same at supersonic and subsonic speeds. At supersonic speeds (e.g., at  $M = 4.0$ ), the angle of attack for best  $L/D$  and/or best  $(L/D)I$  is relatively large, about  $6^\circ$ . Although the angle of attack for best  $L/D$  is lower at subsonic speeds, the large engine size required for supersonic speeds makes the best  $(L/D)I$  at subsonic speed occur at high altitude with corresponding high angles of attack to avoid excess throttling of the engine with the corresponding low specific impulses.

Equation (J5) becomes

$$-\frac{d_e}{c} = \frac{1}{\frac{1}{(L/D)_p} - \frac{1}{(L/D)_b}} \quad (J6)$$

For the case considered in the ANALYSIS AND DISCUSSION ( $(L/D)_b = \infty$ ), the assumption that  $\alpha_b = \alpha_p$  is not required, and equation (J6) becomes

$$-\frac{d_e}{c} = \left(\frac{L}{D}\right)_p \quad (J7)$$

#### Case II

In case II, the inlet momentum is used to counteract the wing center-of-pressure shift. Assuming that  $d_D = 0$ ,  $d_e = 0$ , and  $\alpha_p = \alpha_b$ , equation (J5) becomes

$$\frac{d_{in} - l_{in} \sin \alpha}{c} = -\frac{1}{\left(\frac{\Phi_{in}}{W_G}\right)_p - \left(\frac{\Phi_{in}}{W_G}\right)_b} \quad (J8)$$

The term  $\Phi_{in}/W_G$  is determined by equations (D5) and (D10). For the case considered in the ANALYSIS AND DISCUSSION  $((L/D)_b = \infty)$ , the assumption that  $\alpha_b = \alpha_p$  is not required, and equation (J8) becomes

$$\frac{d_{in} - l_{in} \sin \alpha}{c} = - \frac{1}{\left(\frac{\Phi_{in}}{W_G}\right)_p} \quad (J9)$$

## Case III

For case III, the exit momentum is used to counteract the wing center-of-pressure shift, and  $d_{in}$ ,  $l_{in}$ , and  $d_D$  are set equal to zero, so that equation (J5) becomes

$$- \frac{d_e}{c} = \frac{1}{\left(\frac{\Phi_e}{W_G}\right)_p - \left(\frac{\Phi_e}{W_G}\right)_b} \quad (J10)$$

The term  $\Phi_e/W_G$  is determined by equations (D5) and (D9). For the case considered in the ANALYSIS AND DISCUSSION  $((L/D)_b = \infty)$ , equation (J10) becomes

$$- \frac{d_e}{c} = \frac{1}{\left(\frac{\Phi_e}{W_G}\right)_p} \quad (J11)$$

The angle of jet cant for trim  $\theta$  discussed in appendix I is related to the jet offset  $d_e$  in case III by the relation

$$\sin \theta \approx \tan \theta = \frac{d_e}{t}$$

In an actual airplane a combination of these cases would likely be used to minimize the effect of wing center-of-pressure shift.

## APPENDIX K

## EFFECT ON RANGE OF USING AIRFRAME BOUNDARY LAYER IN ENGINE

The use of airframe boundary layer in the engine cycle is considered in this appendix. The airplane components such as wing and engine are assumed fixed in size. The change in range is calculated from the change in engine performance only. The airplane flight altitude and lift-drag ratio stay constant, so the logarithmic differentiation of the range equation yields

$$\frac{dR}{R} = \left( \frac{dI}{I} \right)_{\Delta C_F=0} \quad (K1)$$

where the required engine thrust coefficient stays constant as indicated.

Consider first the general effect of ingesting the airframe boundary layer on engine thrust and specific impulse; second, consider the effect on airplane range. The nomenclature used in this development is shown in figure 27. The static pressure at the engine inlet is assumed equal to free-stream static pressure. Therefore, the momentum in the boundary layer is characterized by its total pressure  $P_{in}$ . The engine specific impulse and thrust coefficient may be considered a function of the cycle temperature, inlet pressure recovery, and inlet momentum:

$$I = f(T_7, P_2/P_0, \Phi_{in}) \quad (K2)$$

$$C_F = g(T_7, P_2/P_0, \Phi_{in}) \quad (K3)$$

Differentiating equations (K2) and (K3) with respect to  $P_{in}/P_0$  gives

$$\frac{dI}{d\left(\frac{P_{in}}{P_0}\right)} = \left[ \left( \frac{\partial I}{\partial T_7} \right) \frac{\partial T_7}{\partial C_F} \frac{\partial C_F}{\partial \left(\frac{P_{in}}{P_0}\right)} \right]_{P_2/P_0, \Phi_{in}} + \left[ \frac{\partial I}{\partial \left(\frac{P_2}{P_0}\right)} \right]_{T_7, \Phi_{in}} \frac{d\left(\frac{P_2}{P_0}\right)}{d\left(\frac{P_{in}}{P_0}\right)} + \left( \frac{\partial I}{\partial \Phi_{in}} \right)_{T_7, P_2/P_0} \frac{d\Phi_{in}}{d\left(\frac{P_{in}}{P_0}\right)} \quad (K4)$$

$$0 = \frac{dC_F}{d\left(\frac{P_{in}}{P_0}\right)} = \left[ \left( \frac{\partial C_F}{\partial T_7} \right) \frac{\partial T_7}{\partial C_F} \frac{\partial C_F}{\partial \left(\frac{P_{in}}{P_0}\right)} \right]_{P_2/P_0, \Phi_{in}} + \left[ \frac{\partial C_F}{\partial \left(\frac{P_2}{P_0}\right)} \right]_{T_7, \Phi_{in}} \left[ \frac{d\left(\frac{P_2}{P_0}\right)}{d\left(\frac{P_{in}}{P_0}\right)} \right] + \left( \frac{\partial C_F}{\partial \Phi_{in}} \right)_{T_7, P_2/P_0} \left[ \frac{d\Phi_{in}}{d\left(\frac{P_{in}}{P_0}\right)} \right] \quad (K5)$$

Combining equations (K4) and (K5) gives

$$\frac{dI}{d\left(\frac{P_{in}}{P_0}\right)} = \frac{d\left(\frac{P_2}{P_0}\right)}{d\left(\frac{P_{in}}{P_0}\right)} \left\{ \left[ \frac{\partial I}{\partial \left(\frac{P_2}{P_0}\right)} \right]_{T_7, \Phi_{in}} - \left( \frac{\partial I}{\partial C_F} \right)_{P_2/P_0, \Phi_{in}} \left[ \frac{\partial C_F}{\partial \left(\frac{P_2}{P_0}\right)} \right]_{T_7, \Phi_{in}} \right\} + \frac{d\Phi_{in}}{d\left(\frac{P_{in}}{P_0}\right)} \left[ \left( \frac{\partial I}{\partial \Phi_{in}} \right)_{T_7, P_2/P_0} - \left( \frac{\partial I}{\partial C_F} \right)_{P_2/P_0, \Phi_{in}} \left( \frac{\partial C_F}{\partial \Phi_{in}} \right)_{T_7, P_2/P_0} \right] \quad (K6)$$

From the relation

$$F = \Phi_e - \Phi_{in} \quad (K7)$$

for constant  $P_2/P_0$  (which infers a constant airflow rate  $w_a$ ) and constant  $T_7$  (which infers constant  $w_f/w_a$ ), differentiation yields

$$\left[ \frac{\partial F}{\partial \left(\frac{P_{in}}{P_0}\right)} \right]_{T_7, P_2/P_0} = - \left[ \frac{\partial \Phi_{in}}{\partial \left(\frac{P_{in}}{P_0}\right)} \right]_{T_7, P_2/P_0} \quad (K8)$$

and, using the definition of specific impulse,

$$\begin{aligned}
 \frac{1}{I} \left[ \frac{\partial I}{\partial \left( \frac{P_{in}}{P_0} \right)} \right]_{T_7, P_2/P_0} &= \frac{1}{C_F} \left[ \frac{\partial C_F}{\partial \left( \frac{P_{in}}{P_0} \right)} \right]_{T_7, P_2/P_0} \\
 &= \frac{1}{F} \left[ \frac{\partial F}{\partial \left( \frac{P_{in}}{P_0} \right)} \right]_{T_7, P_2/P_0} \\
 &= - \frac{1}{C_F \frac{\gamma}{2} P_0 M_{O,F}^2 A_0} \left[ \frac{\partial \phi_{in}}{\partial \left( \frac{P_{in}}{P_0} \right)} \right]_{T_7, P_2/P_0} \quad (K9)
 \end{aligned}$$

The change of inlet momentum from the free-stream value due to the intake of boundary layer may be found from

$$\phi_{in} = \gamma P_0 M_{O,F}^2 A_0 \quad (K10)$$

For constant  $P_2/P_0$ , which is assumed to imply constant  $A_0$ , which in turn assumes a constant combustor-inlet Mach number (see ref. 2), differentiation of equation (K10) gives

$$\begin{aligned}
 \left[ \frac{\partial \phi_{in}}{\partial \left( \frac{P_{in}}{P_0} \right)} \right]_{T_7, P_2/P_0} &= 2\gamma P_0 M_{O,F}^2 A_0 \left[ \frac{\partial M_{in}}{\partial \left( \frac{P_{in}}{P_0} \right)} \right]_{P_2/P_0} \\
 &= 2\gamma P_0 M_{O,F}^2 A_0 \frac{dM_{in}}{d \left( \frac{P_{in}}{P_0} \right)} \quad (K11)
 \end{aligned}$$

The term  $dM_{in}/d(P_{in}/P_0)$  may be calculated from existing tables (e.g., ref. 4) by taking increments; results are shown in figure 28. Combining

equations (K9) and (K11) with (K6) gives the general relation

$$\frac{dI}{d\left(\frac{P_{in}}{P_0}\right)} = \frac{d\left(\frac{P_2}{P_0}\right)}{d\left(\frac{P_{in}}{P_0}\right)} \left\{ \left[ \frac{\partial I}{\partial\left(\frac{P_2}{P_0}\right)} \right]_{T_7, \Phi_{in}} - \left( \frac{\partial I}{\partial C_F} \right)_{P_2/P_0, \Phi_{in}} \left[ \frac{\partial C_F}{\partial\left(\frac{P_2}{P_0}\right)} \right]_{T_7, \Phi_{in}} \right\} - \frac{4}{M_0} \frac{dM_{in}}{d\left(\frac{P_{in}}{P_0}\right)} \frac{A_0}{A_F} \left[ \frac{I}{C_F} - \left( \frac{\partial I}{\partial C_F} \right)_{P_2/P_0, \Phi_{in}} \right] \quad (KL2)$$

The effect on engine thrust coefficient at constant cycle temperature may be determined from equation (K5) for  $dT_7 = 0$ :

$$\left[ \frac{dC_F}{d\left(\frac{P_{in}}{P_0}\right)} \right]_{T_7=\text{const}} = \left[ \frac{\partial C_F}{\partial\left(\frac{P_2}{P_0}\right)} \right]_{T_7, \Phi_{in}} \frac{d\left(\frac{P_2}{P_0}\right)}{d\left(\frac{P_{in}}{P_0}\right)} - \frac{4}{M_0} \frac{dM_{in}}{d\left(\frac{P_{in}}{P_0}\right)} \frac{A_0}{A_F} \quad (KL2a)$$

Several assumptions may be made with regard to the term  $d(P_2/P_0)/d(P_{in}/P_0)$ . From figure 27,

$$\frac{P_2}{P_0} = \frac{P_2}{P_{in}} \frac{P_{in}}{P_0}$$

It might be argued that, because reducing  $P_{in}$  reduces  $M_{in}$ ,  $P_2/P_0$  is independent of the breakdown of the losses between stations 0 and 2, in which case

$$\frac{d\left(\frac{P_2}{P_0}\right)}{d\left(\frac{P_{in}}{P_0}\right)} = 0 \quad (KL3)$$

and it is clearly advantageous to use the boundary layer in the engine. A more conservative assumption is that  $P_2/P_{in}$  is constant at the value

that would exist for no boundary-layer ingestion; in this case,

$$\frac{d\left(\frac{P_2}{P_0}\right)}{d\left(\frac{P_{in}}{P_0}\right)} = \frac{P_2}{P_0} \quad (K14)$$

The change in range may be written from (K1),

$$\frac{\Delta R}{R} = \frac{1}{I} \left[ \frac{dI}{d\left(\frac{P_{in}}{P_0}\right)} \right] \Delta\left(\frac{P_{in}}{P_0}\right) \quad (K15)$$

where  $\Delta(P_{in}/P_0)$  may be evaluated from the friction drag on the airplane. Using equation (K10) for the inlet momentum, for a given stream tube of air  $A_0$ ,

$$\Delta\left(\frac{P_{in}}{P_0}\right) = \frac{\Delta P_{in}}{P_0} = \frac{\Delta\Phi_{in}}{2\gamma P_0 M_0 A_0 \left[ \frac{dM_{in}}{d\left(\frac{P_{in}}{P_0}\right)} \right]} \quad (K16)$$

where the change in inlet momentum (momentum at the engine inlet  $\Phi_{in}$  minus the free-stream momentum  $\Phi_0$ ) is the momentum defect resulting from taking boundary-layer air into the engine. Thus, letting  $D_{fr}$  equal the total friction drag, and  $\eta$  the fraction of the momentum defect ingested,

$$\Delta\Phi_{in} = \eta D_{fr} \quad (K17)$$

In terms of the fraction of airplane drag at zero lift that is friction, by using the relation given by equation (C20) and the fact that

$F = D = C_F \frac{\gamma}{2} \rho_0 M_0^2 A_F$ , the following is obtained:

$$\frac{\Delta P_{in}}{P_0} = - \frac{C_{D,o,fr} \eta}{C_{D,o} \left( 1 + \frac{1}{C} \right)} \frac{M_0 C_F}{\frac{dM_{in}}{d\left(\frac{P_{in}}{P_0}\right)} \frac{A_0}{A_F}} \quad (K18)$$

In equation (K18) the term  $A_0/A_F$  may be taken as that for the engine using free-stream air. These values are given in reference 2. Accounting for the reduction in  $A_0/A_F$  because of the reduced inlet pressure recovery  $P_2/P_0$  introduces a second-order correction that further amplifies the effect of using the boundary layer in the engine. Combining equations (K18), (K15), (K14), and (K12) yields the final result:

$$\frac{\Delta R}{R} = \frac{1}{C_F} \left( \frac{P_2}{P_0} \frac{C_F}{I} \left\{ \left[ \frac{\partial I}{\partial \left( \frac{P_2}{P_0} \right)} \right]_{T_7, \Phi_{in}} - \left( \frac{\partial I}{\partial C_F} \right)_{P_2/P_0, \Phi_{in}} \left[ \frac{\partial C_F}{\partial \left( \frac{P_2}{P_0} \right)} \right]_{T_7, \Phi_{in}} \right\} - \frac{4}{M_0} \frac{dM_{in}}{d \left( \frac{P_{in}}{P_0} \right)} \frac{A_0}{A_F} \right) \left[ \frac{\left( \frac{C_{D,o_{fr}}}{C_{D,o}} \right) \eta C_F}{1 + \frac{1}{C}} \frac{M_0}{4 \frac{A_0}{A_F} \frac{dM_{in}}{d \left( \frac{P_{in}}{P_0} \right)}} \right] \quad (K19)$$

and, from equation (K12a) at constant cycle temperature,

$$\frac{\Delta C_F}{C_F} = \frac{1}{C_F} \left\{ \left[ \frac{\partial C_F}{\partial \left( \frac{P_2}{P_0} \right)} \right]_{T_7, \Phi_{in}} \frac{P_2}{P_0} - \frac{4}{M_0} \frac{A_0}{A_F} \frac{dM_{in}}{d \left( \frac{P_{in}}{P_0} \right)} \right\} \left[ \frac{\frac{C_{D,o_{fr}}}{C_{D,o}} \eta C_F M_0}{1 + \frac{1}{C} \frac{4}{A_F} \frac{dM_{in}}{d \left( \frac{P_{in}}{P_0} \right)}} \right] \quad (K20)$$

[Note in comparing the symbols of this appendix with those of ref. 2 that  $(\partial I / \partial C_F)_{P_2/P_0, \Phi_{in}} = (\partial I / \partial C_F)_{X, C_D}$  and  $[(\partial I) / (\partial P_2/P_2)]_{T_7, \Phi_{in}} = (\partial I / \partial P)_{X, C_D}$ .]

REFERENCES

1. Luskin, Harold, and Klein, Harold: The Influence of Turbojet Airflow on the Aerodynamic Design of Airplanes. Rep. No. SM-19111, Santa Monica Div., Douglas Aircraft Co., June 1955.
2. Weber, Richard J., and Luidens, Roger W.: A Simplified Method for Evaluating Jet-Propulsion-System Components in Terms of Airplane Performance. NACA RM E56J26, 1956.

3. Moeckel, W. E., and Connors, J. F.: Charts for the Determination of Supersonic Air Flow Against Inclined Planes and Axially Symmetric Cones. NACA TN 1373, 1947.
4. Ames Research Staff: Equations, Tables, and Charts for Compressible Flow. NACA Rep. 1135, 1953. (Supersedes NACA TN 1428.)

~~CONFIDENTIAL~~

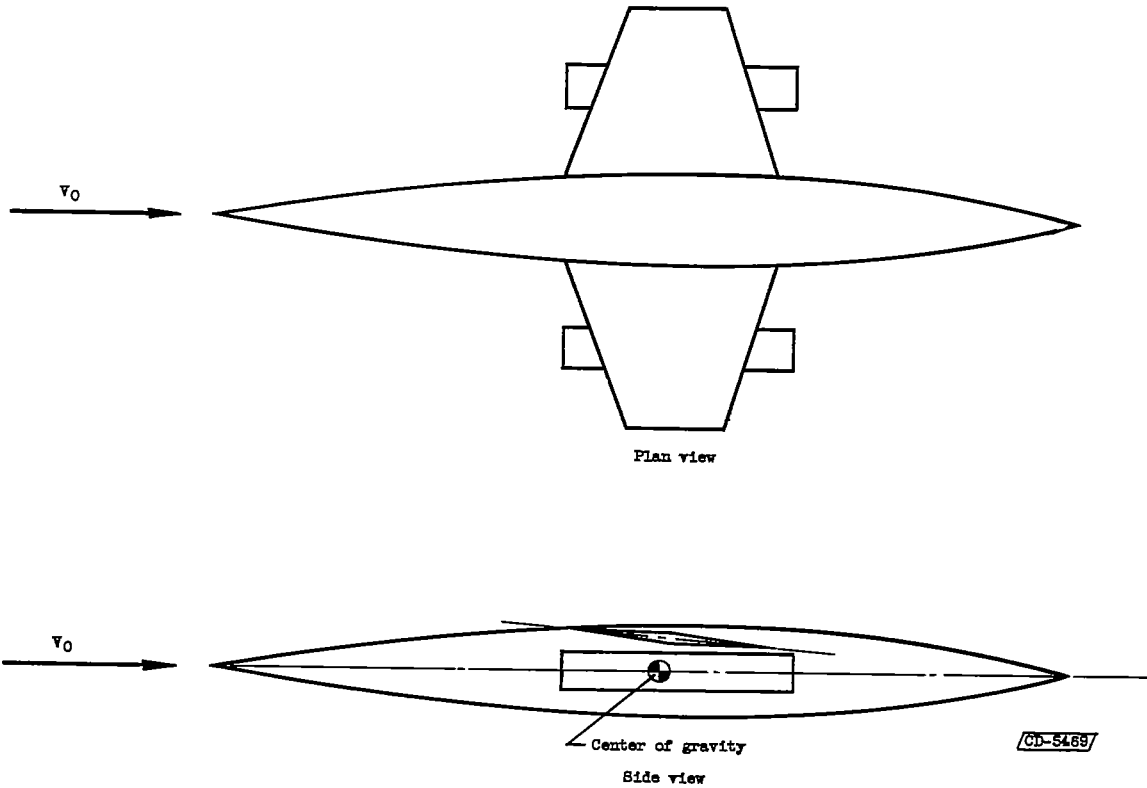


Figure 1. - Schematic arrangement of reference airplane.

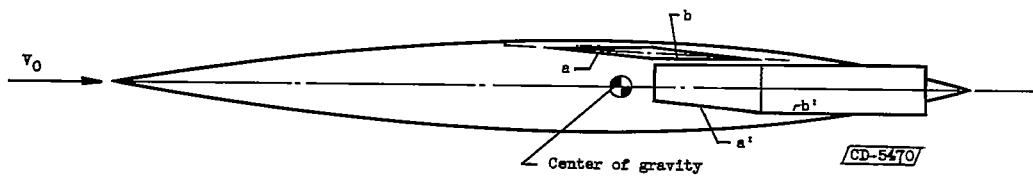
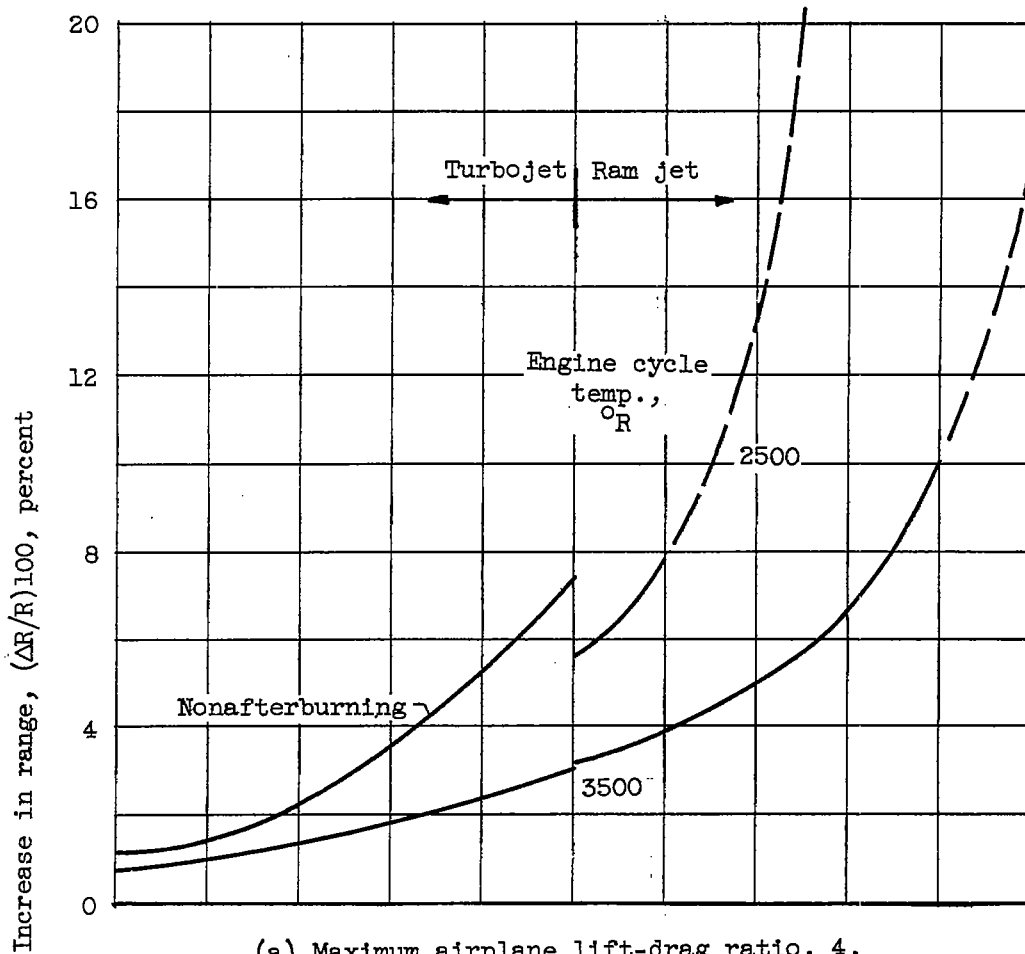
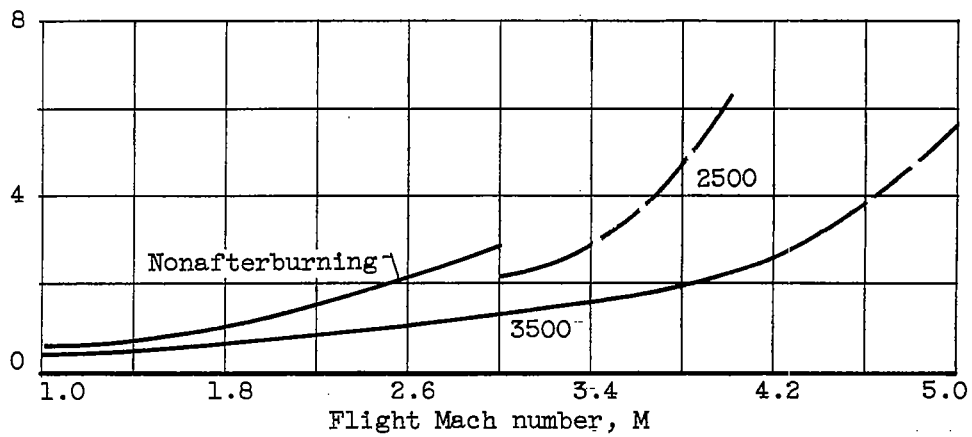


Figure 2. - Schematic arrangement of airplane with inlet located under wing.

~~CONFIDENTIAL~~

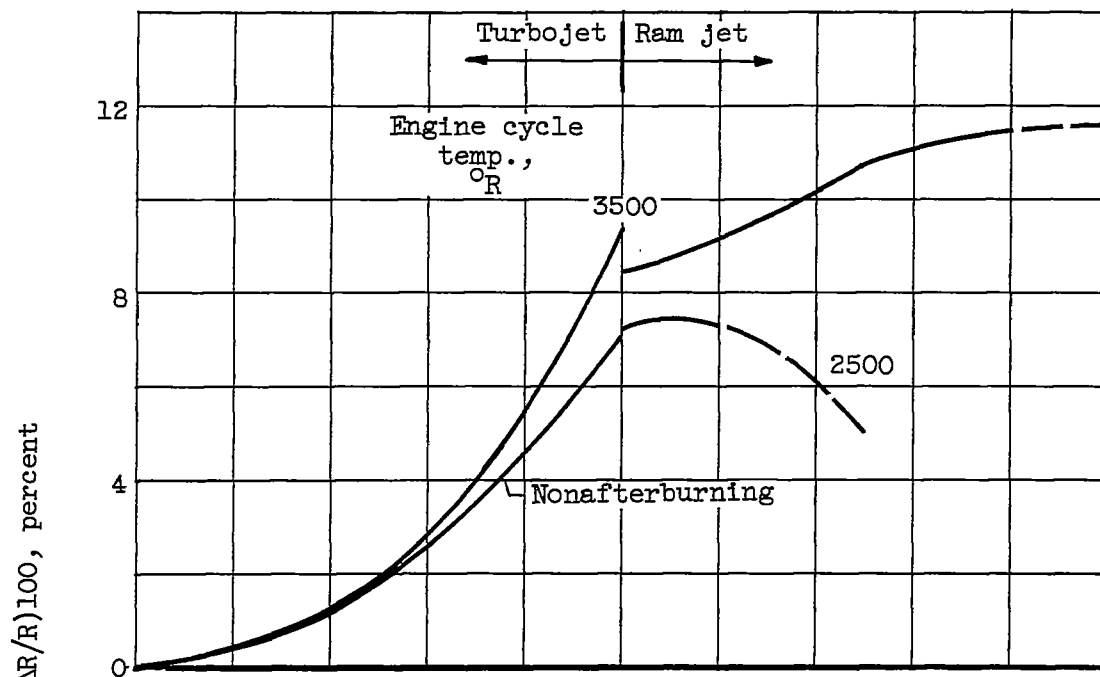


(a) Maximum airplane lift-drag ratio, 4.

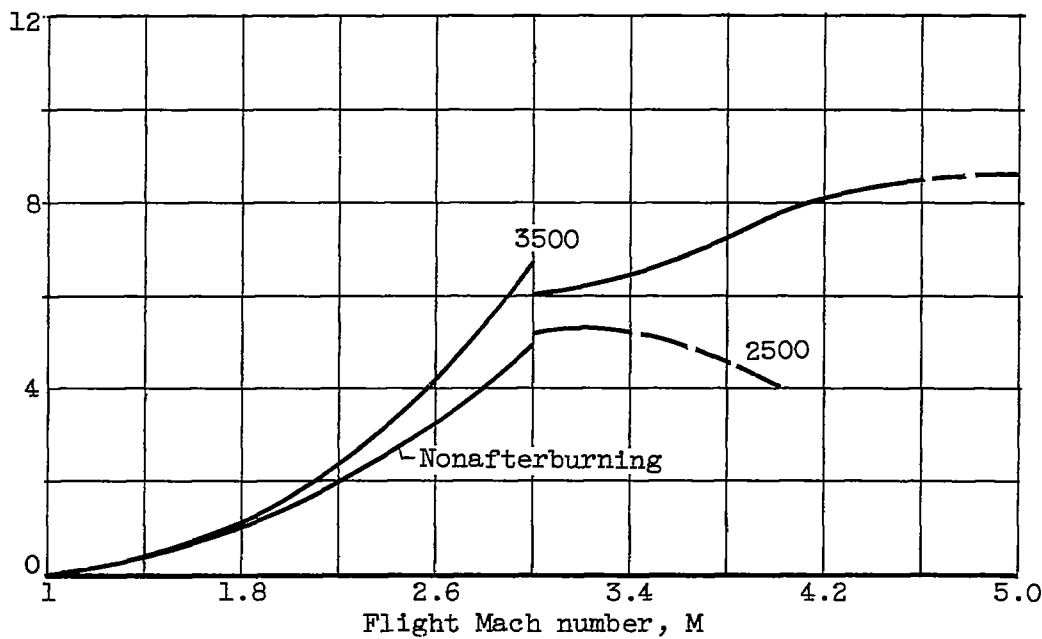


(b) Maximum airplane lift-drag ratio, 8.

Figure 3. - Percent airplane range increase due to reduced engine-inlet momentum under the wing.



(a) Maximum airplane lift-drag ratio, 4.



(b) Maximum airplane lift-drag ratio, 8.

Figure 4. - Percent airplane range increase due to increased pressure recovery under wing.

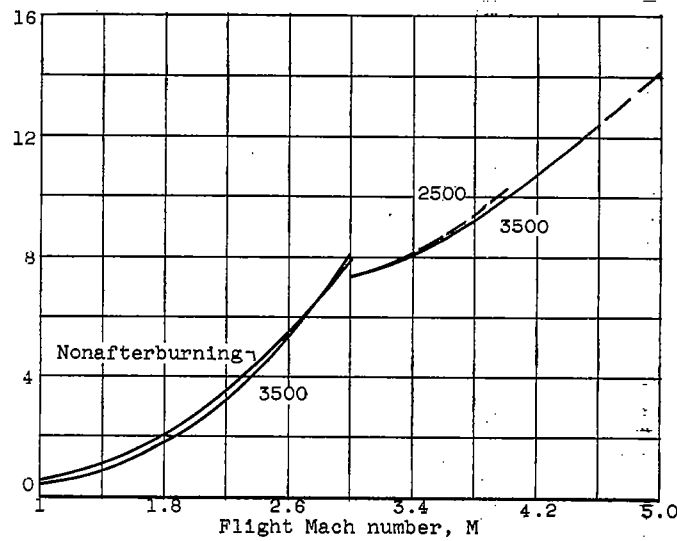
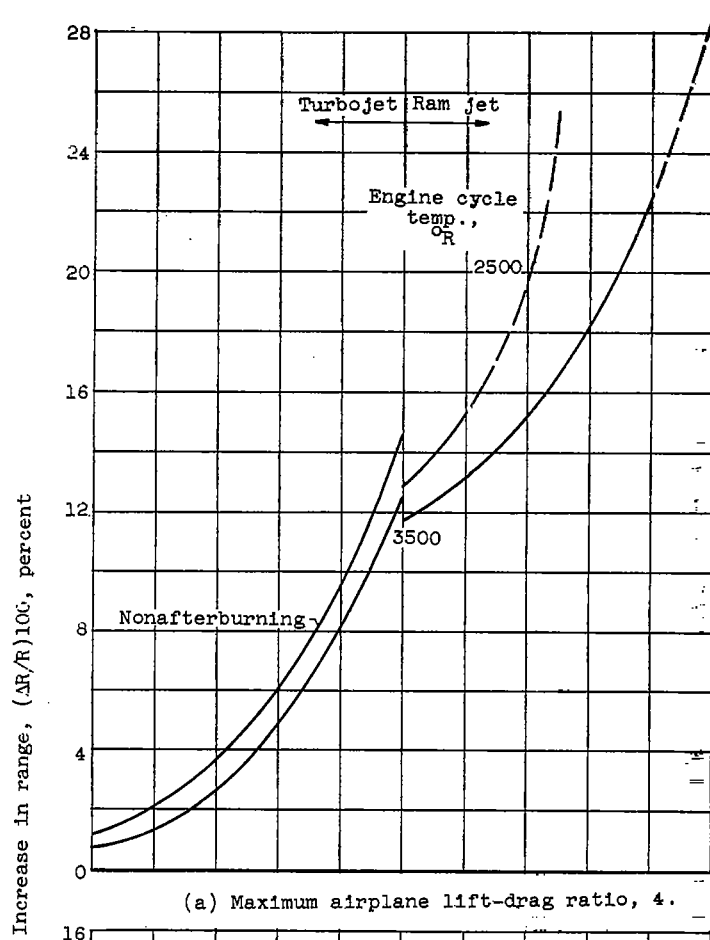


Figure 5. - Percent airplane range increase due to inlet location under wing.

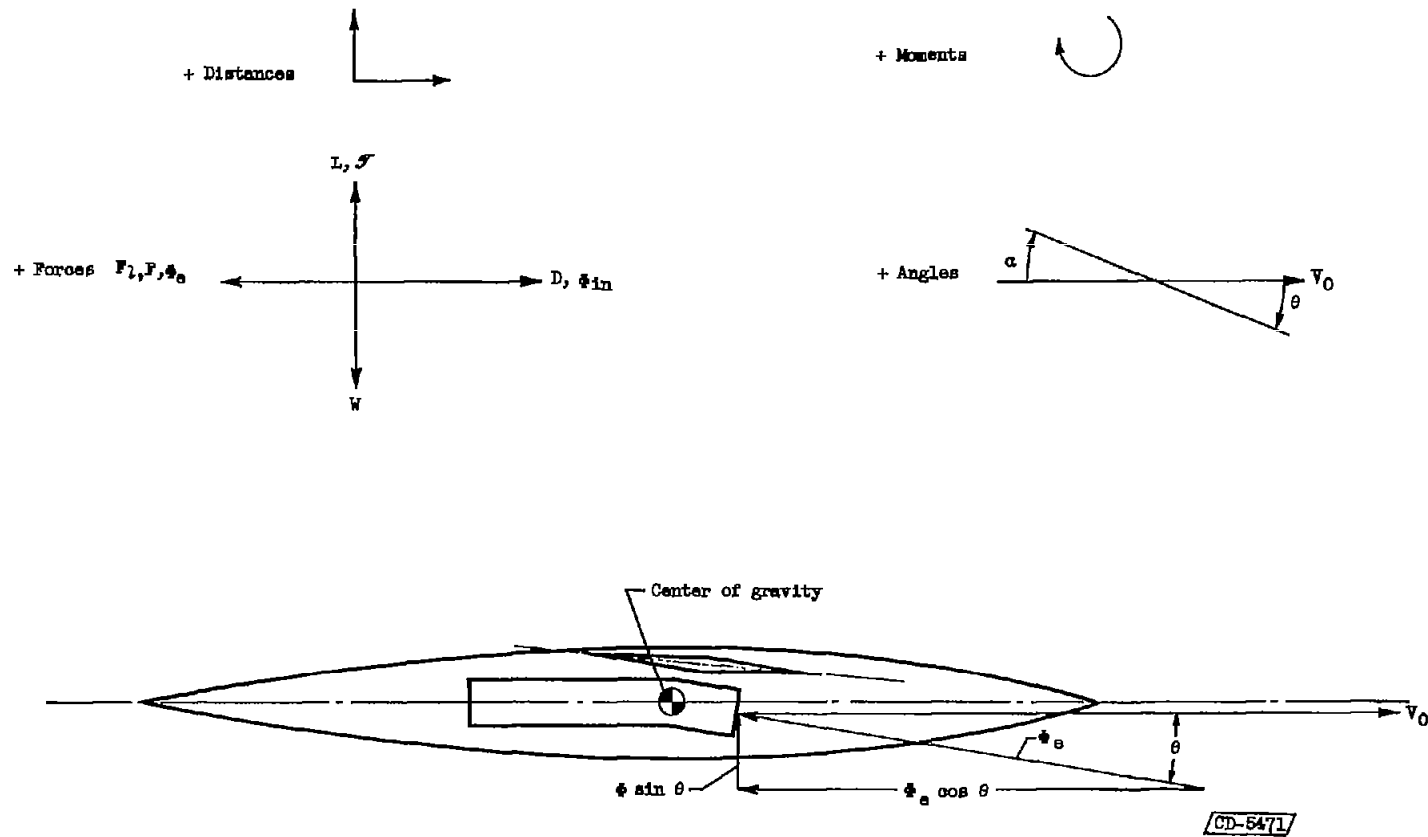
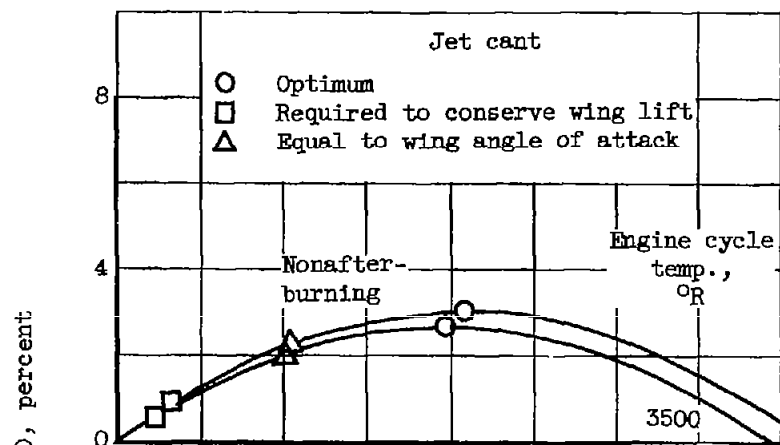
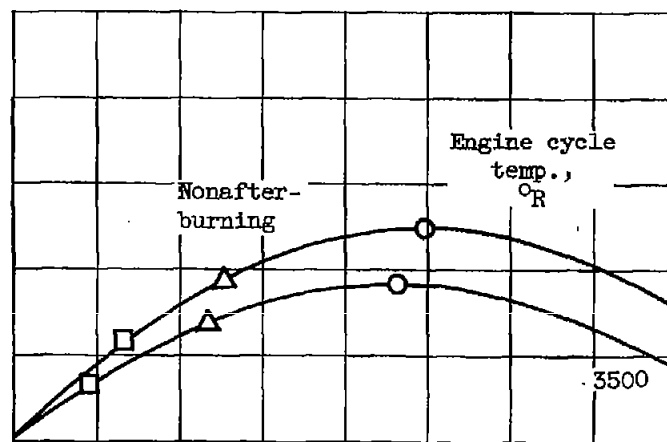


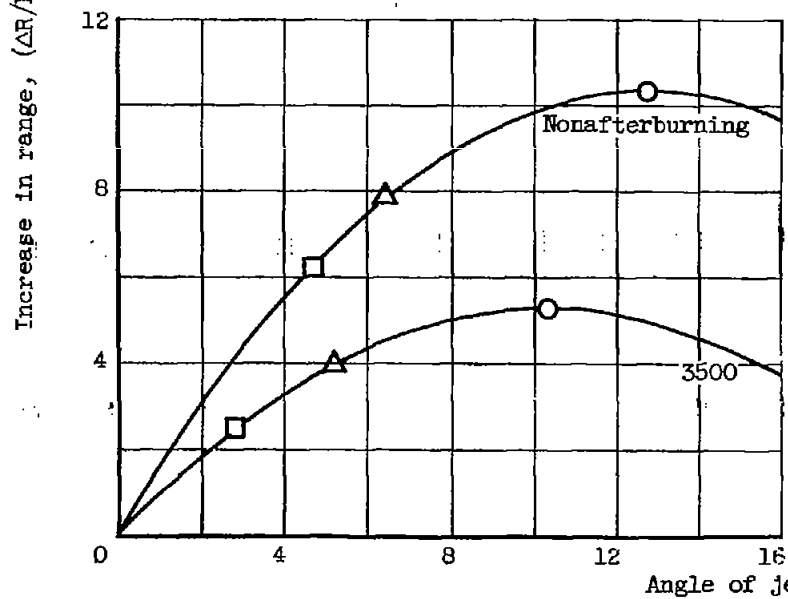
Figure 6. - Schematic arrangement of airplane using jet cant for lift.



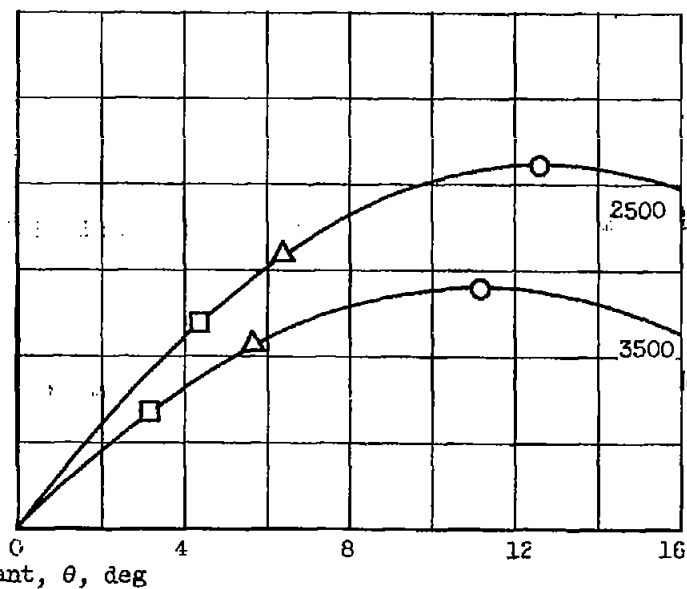
(a) Turbojet; flight Mach number, 1.0.



(b) Turbojet; flight Mach number, 2.0.



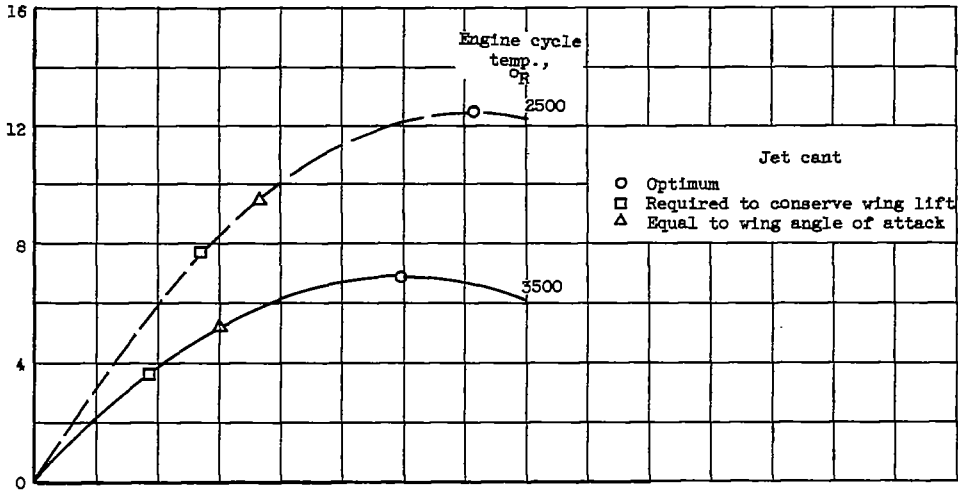
(c) Turbojet; flight Mach number, 3.0.



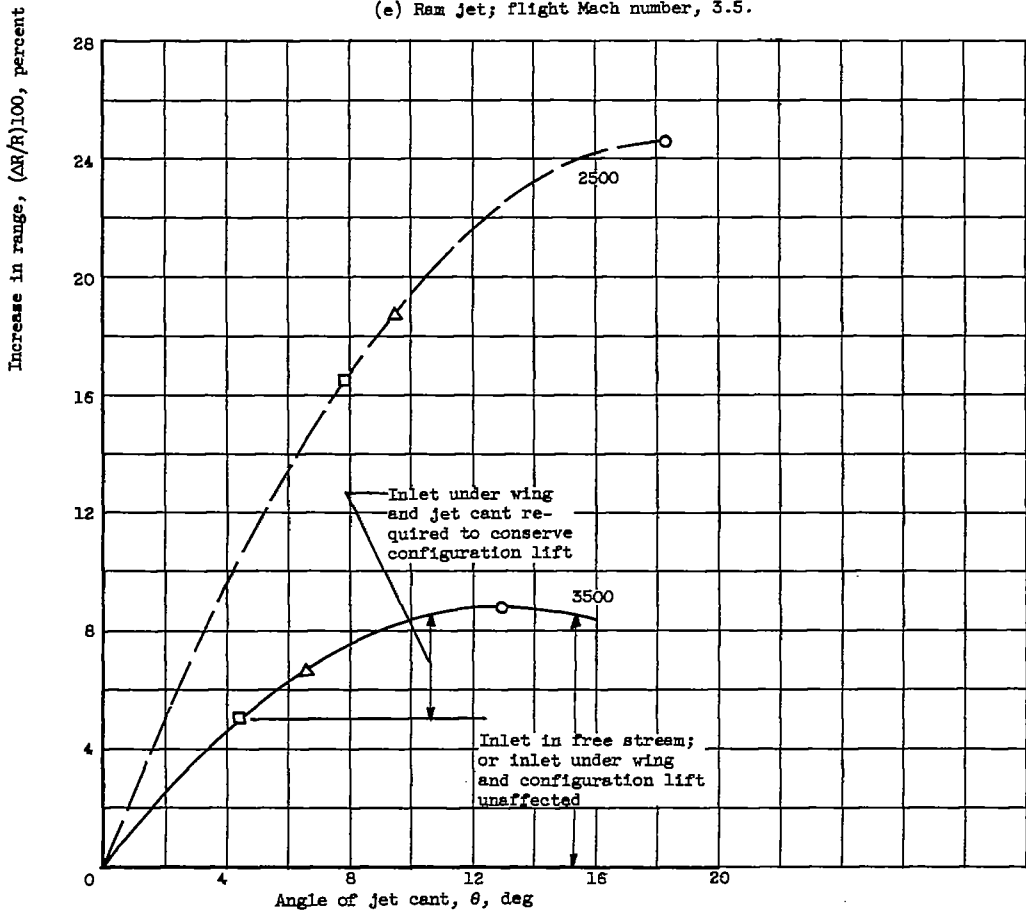
(d) Ram jet; flight Mach number, 3.0.

Figure 7. - Percent airplane range increase due to jet cant for lift. Maximum airplane lift-drag ratio, 4.

~~CONFIDENTIAL~~



(e) Ram jet; flight Mach number, 3.5.



(f) Ram jet; flight Mach number, 4.0.

Figure 7. - Concluded. Percent airplane range increase due to jet cant for lift. Maximum airplane lift-drag ratio, 4.

~~CONFIDENTIAL~~

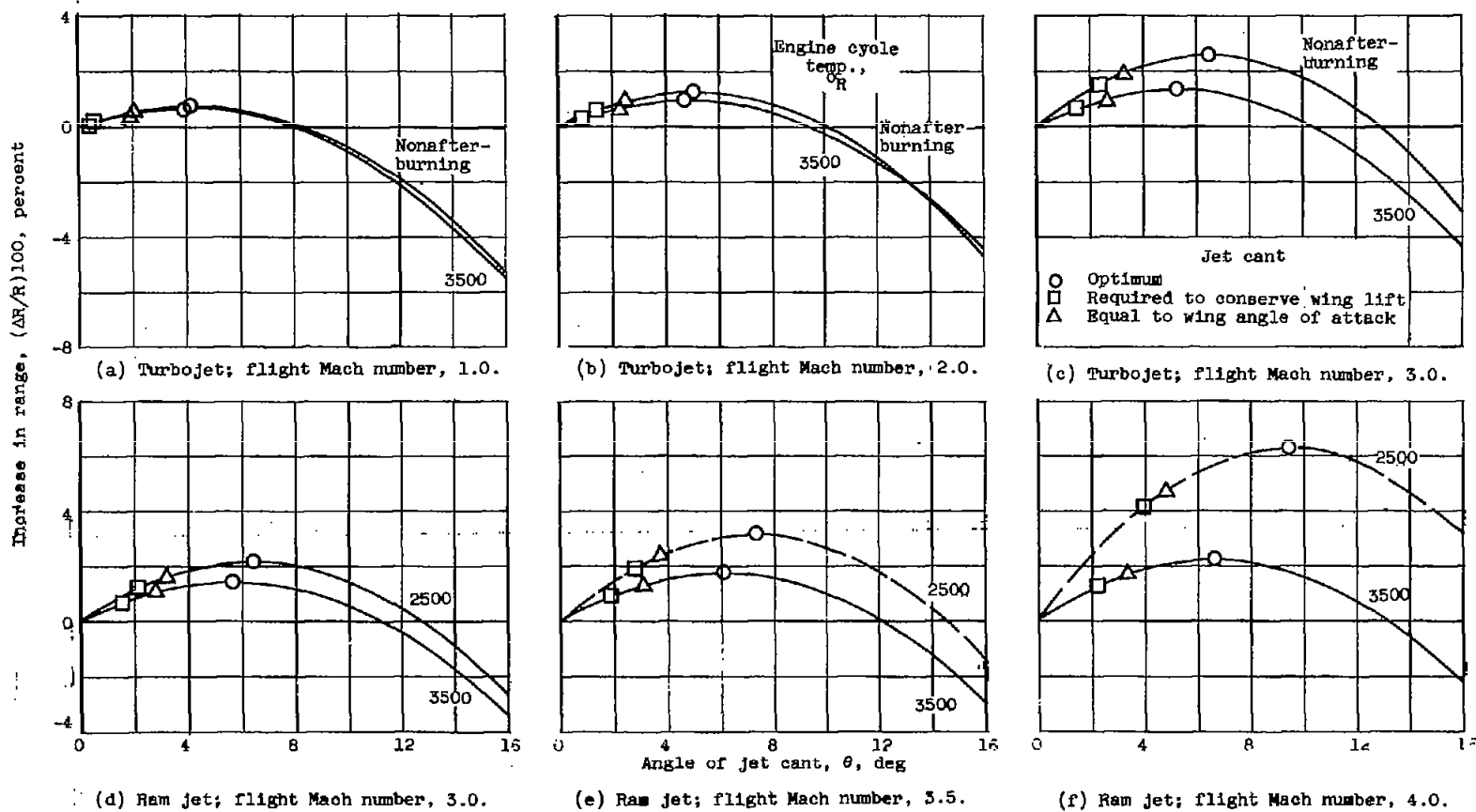
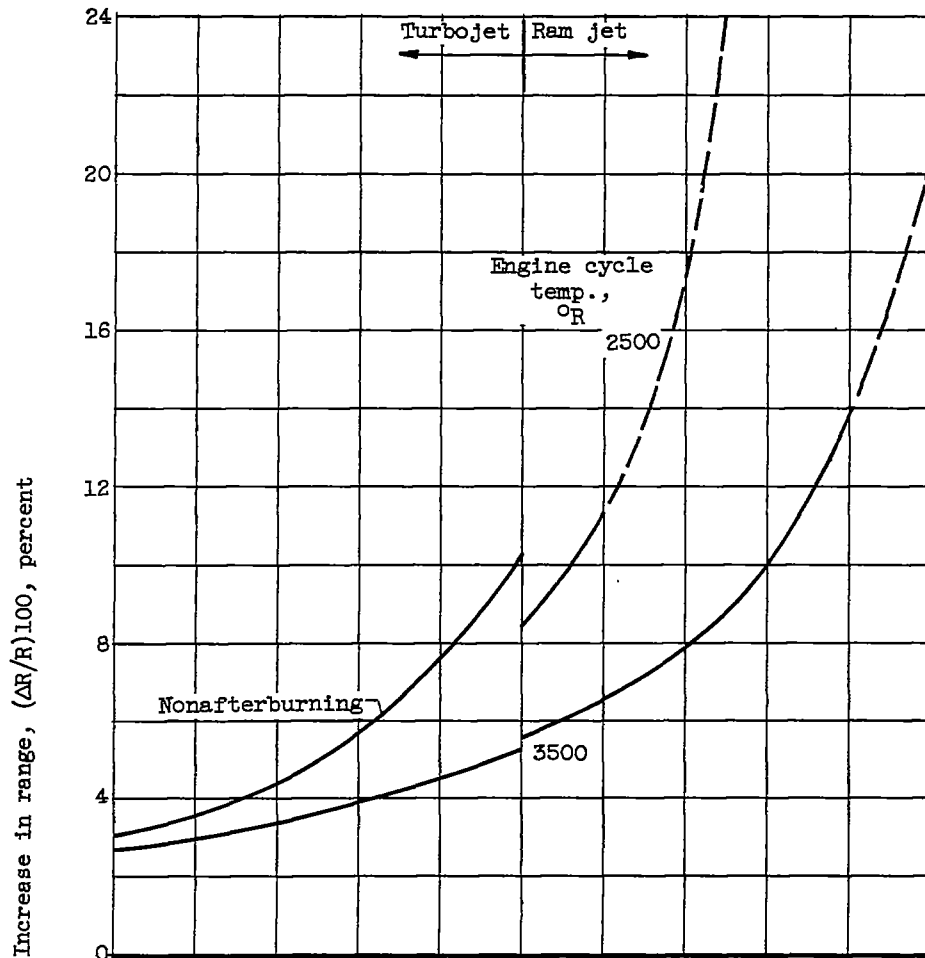
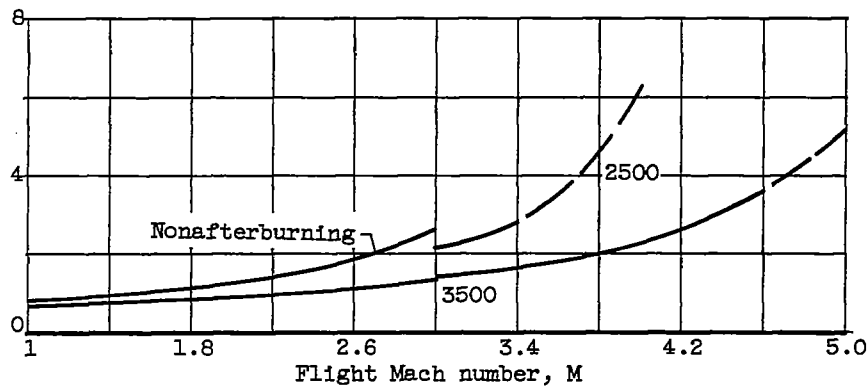


Figure 8. - Percent airplane range increase due to jet cant for lift. Maximum airplane lift-drag ratio, 8.

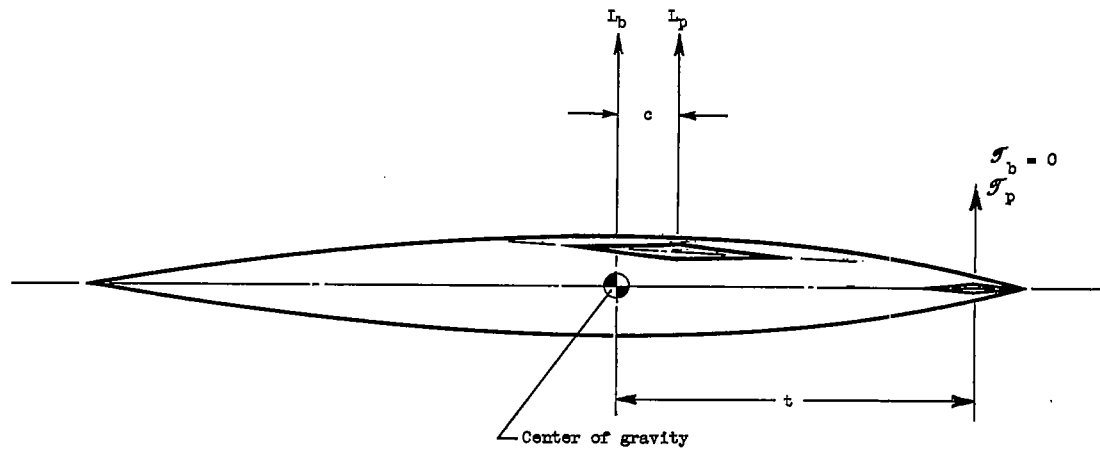


(a) Maximum airplane lift-drag ratio, 4.

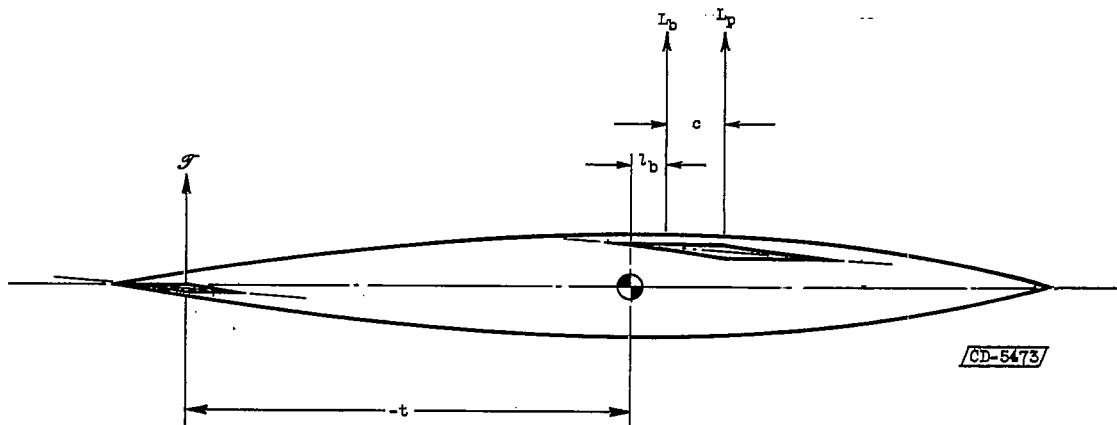


(b) Maximum airplane lift-drag ratio, 8.

Figure 9. - Percent airplane range increase at optimum jet cant; inlet in free stream.

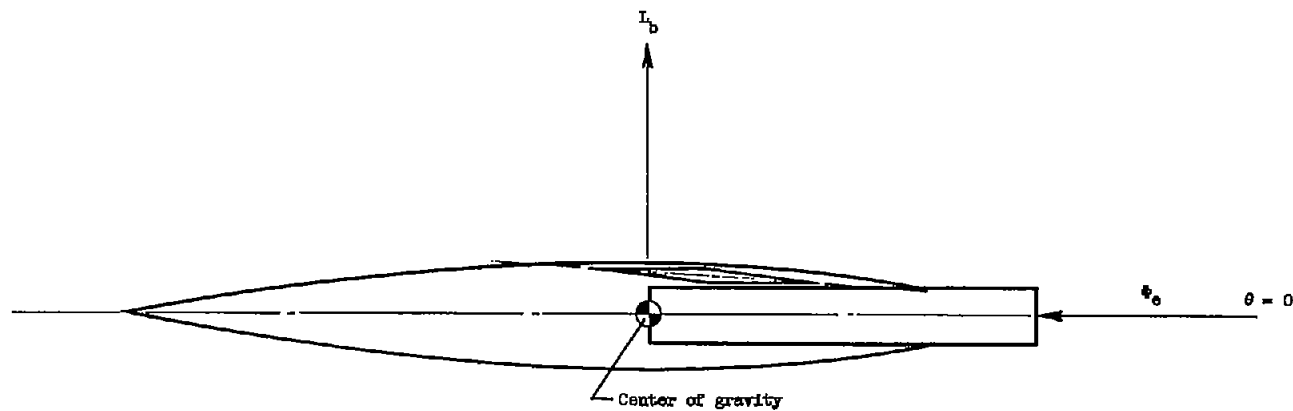


(a) Conventional arrangement.

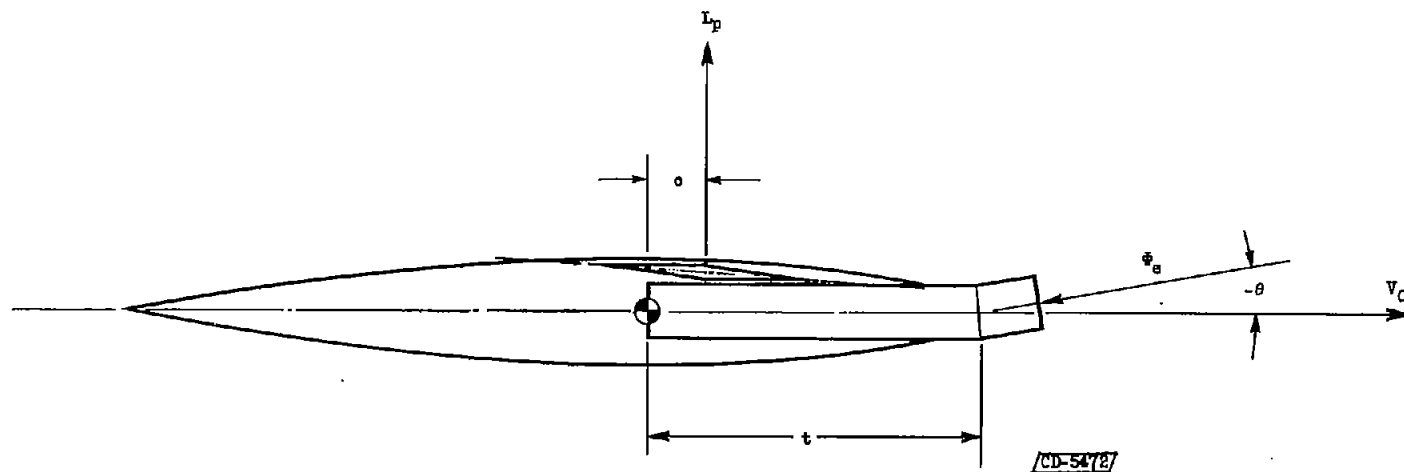


(b) Canard arrangement.

Figure 10. - Schematic airplane arrangements for estimating trim drag. (See fig. 6 for sign conventions.)



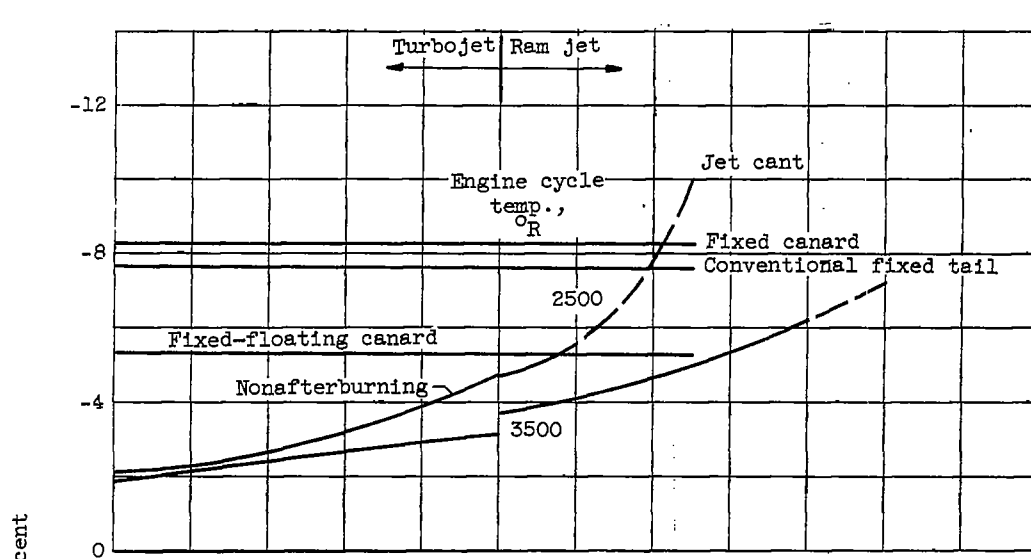
(a) At subsonic speeds.



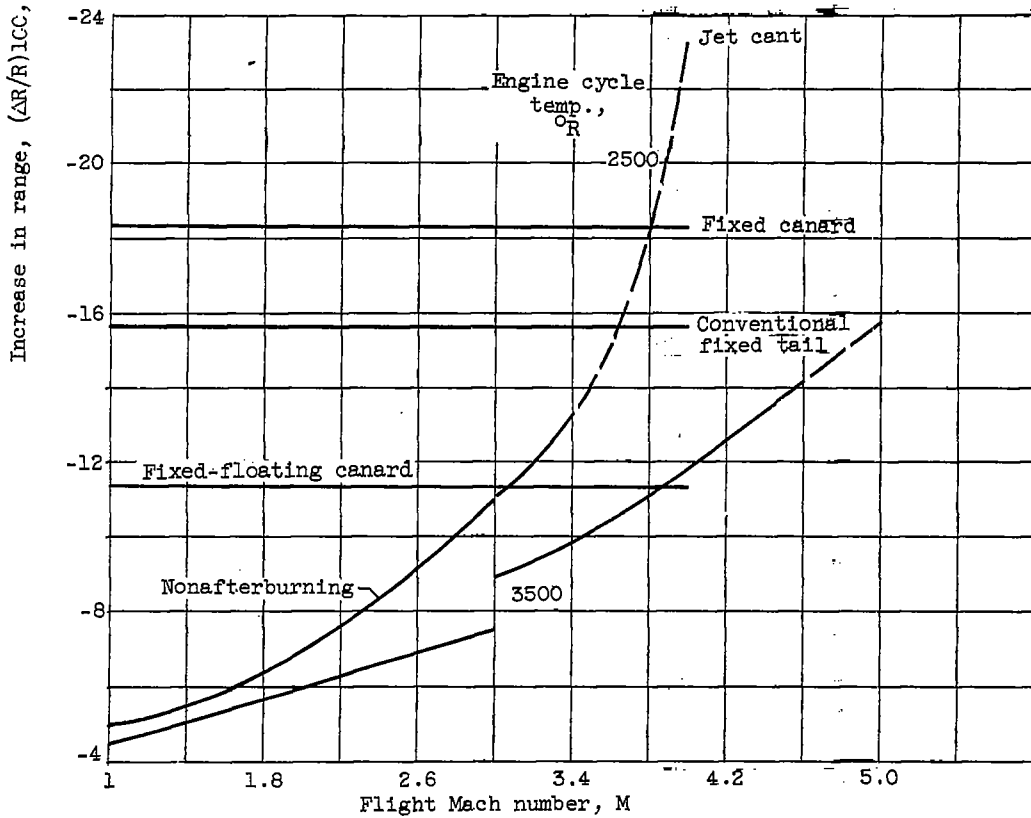
(b) At supersonic speeds.

Figure 11. - Schematic arrangement of airplane using jet cant for trim. (See fig. 6 for sign conventions.)

4077  
CI-9



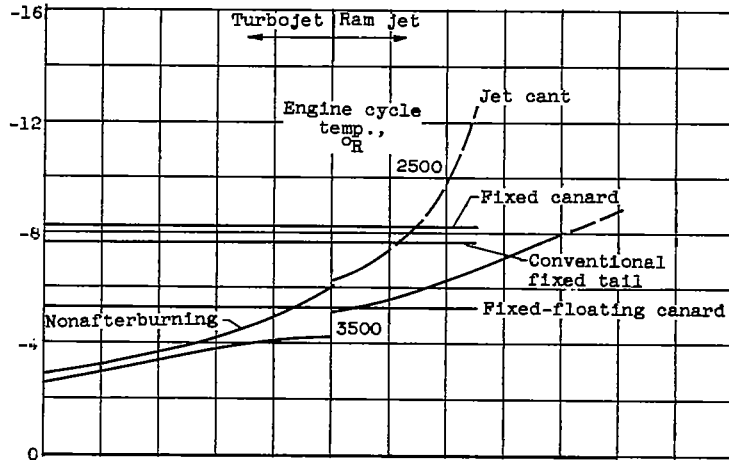
(a) Maximum airplane lift-drag ratio, 4;  $c/t$ , 0.05.



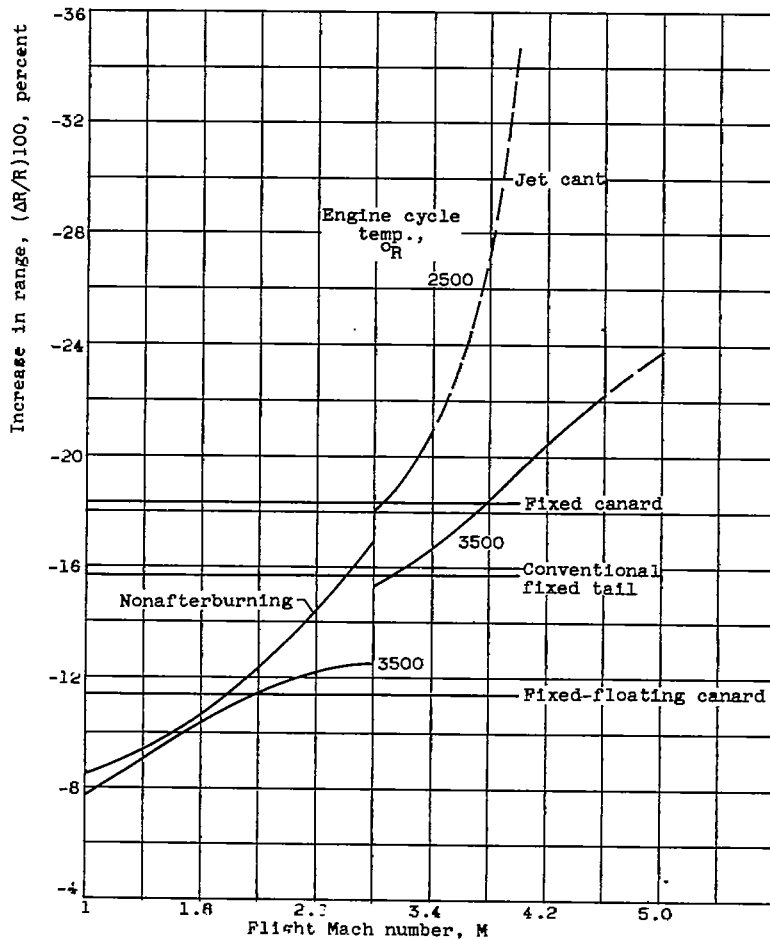
(b) Maximum airplane lift-drag ratio, 4;  $c/t$ , 0.10.

Figure 12. - Percent airplane range increase for several methods of trimming airplane.

4077



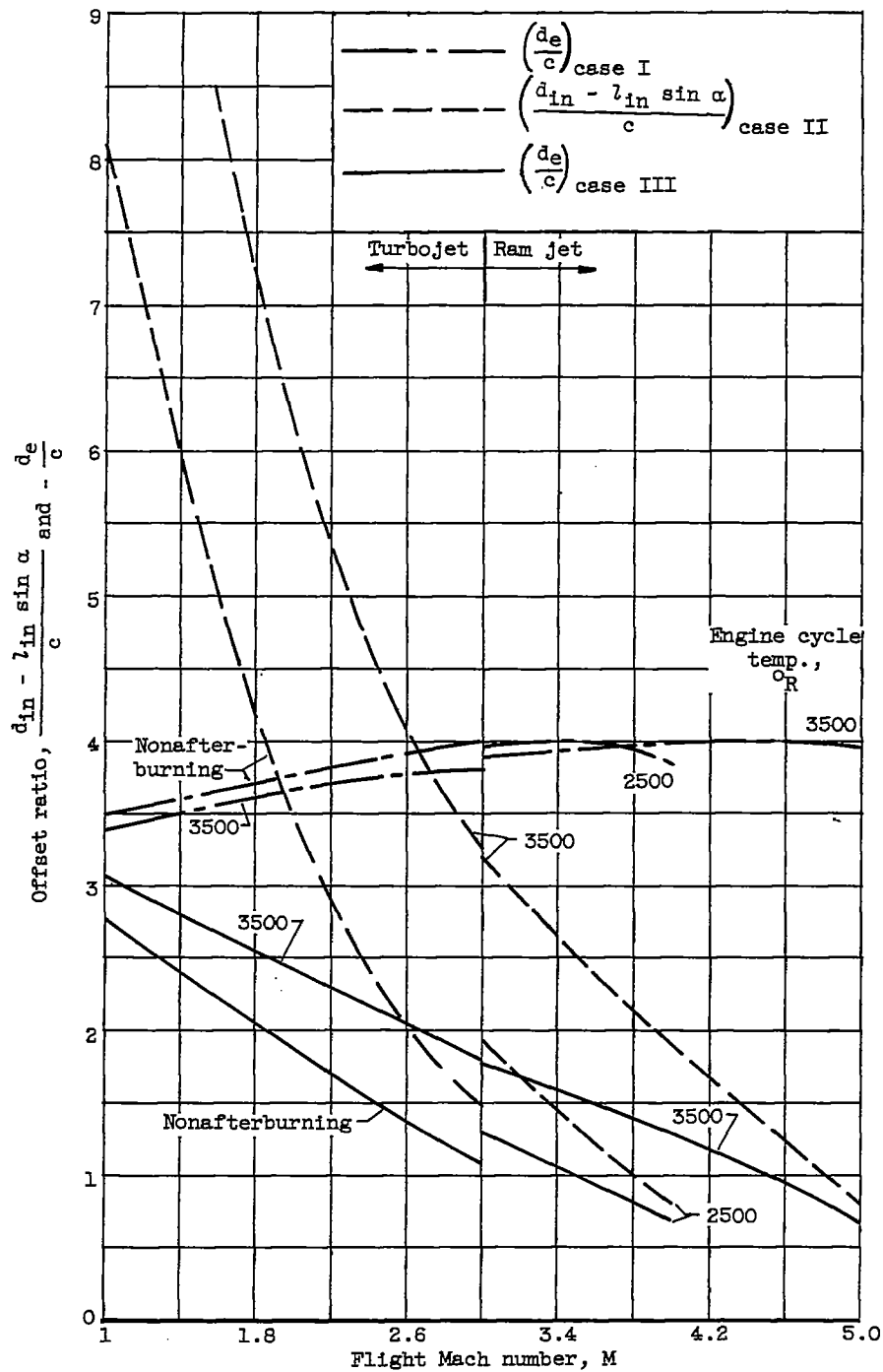
(c) Maximum airplane lift-drag ratio, 8;  $c/t$ , 0.05.



(d) Maximum airplane lift-drag ratio, 8;  $c/t$ , 0.10.

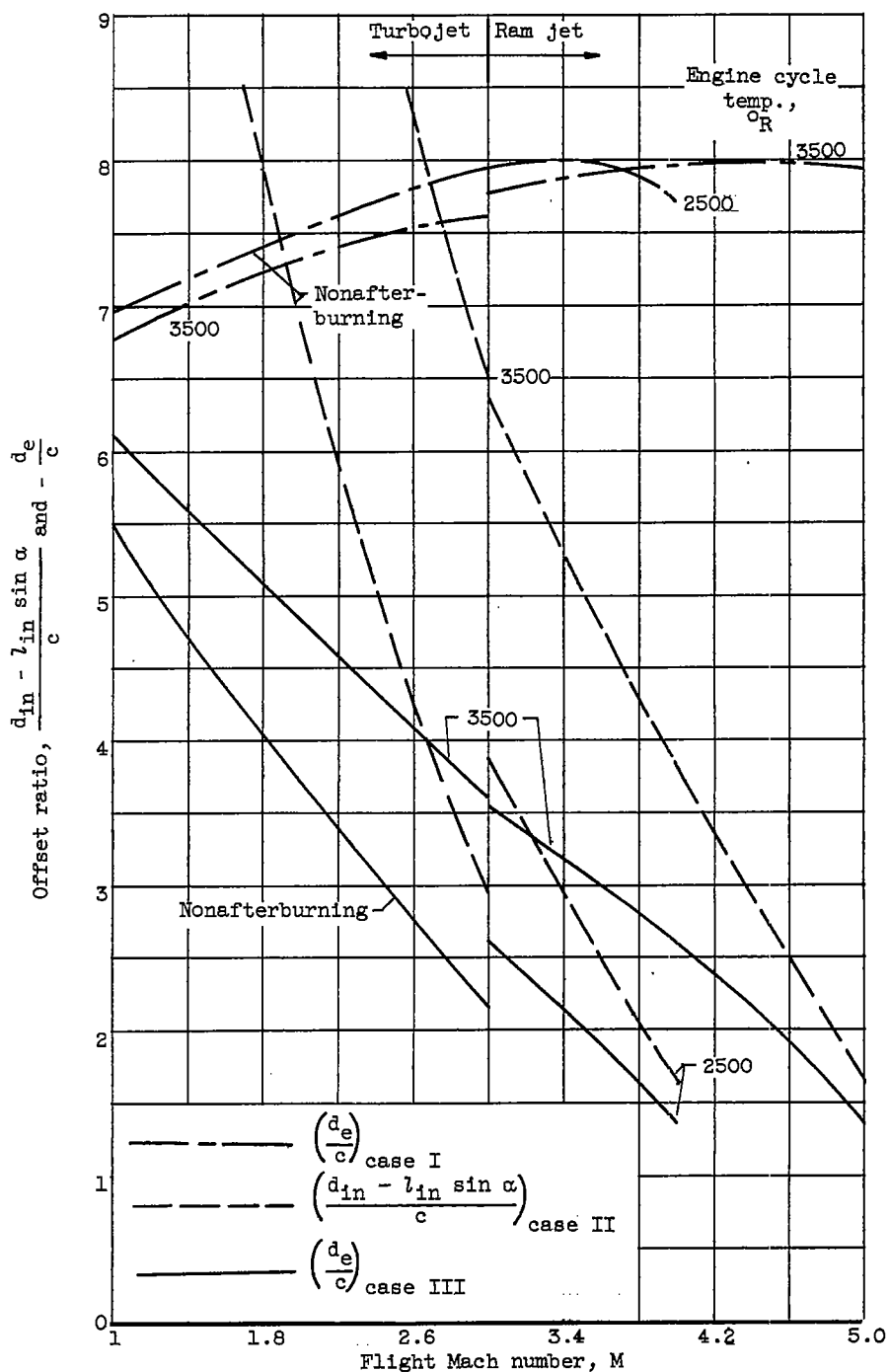
Figure 12. - Concluded. Percent airplane range increase for several methods of trimming airplane.





(a) Maximum airplane lift-drag ratio, 4.

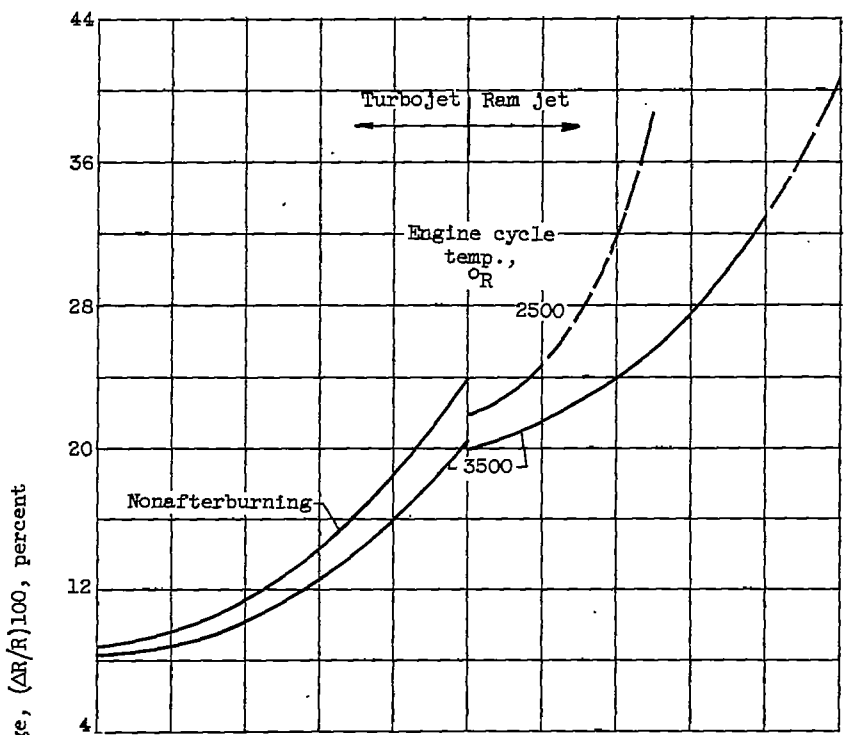
Figure 14. - Engine, or inlet, or exhaust-jet offset required to avoid trim drag. Airplane lift-drag ratio at subsonic speed,  $\infty$ . (See fig. 13 for cases.)



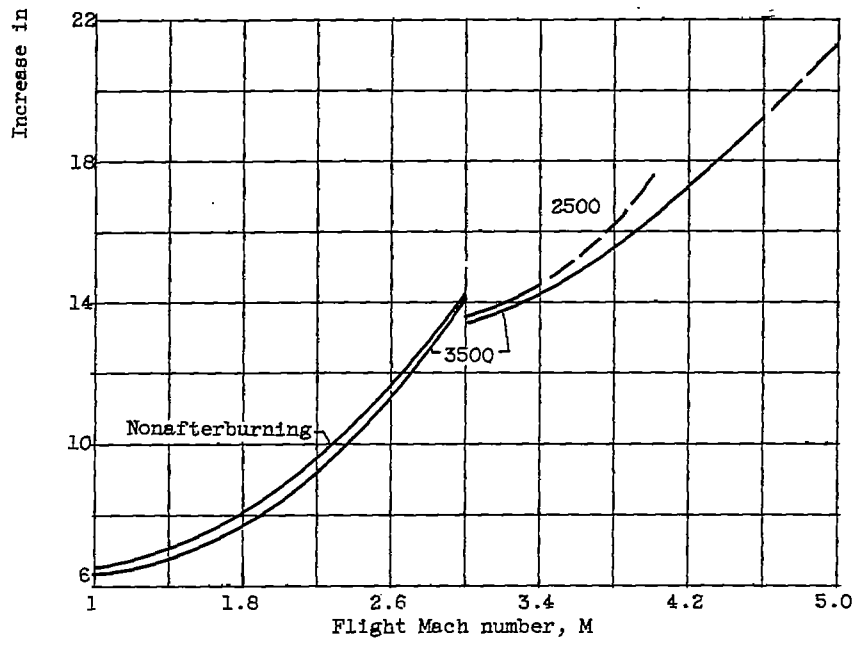
(b) Maximum airplane lift-drag ratio. B.

Figure 14. - Concluded. Engine, or inlet, or exhaust-jet offset required to avoid trim drag. Airplane lift-drag ratio at subsonic speed,  $\infty$ . (See fig. 13 for cases.)

~~CONFIDENTIAL~~



(a) Maximum airplane lift-drag ratio, 4.



(b) Maximum airplane lift-drag ratio, 8.

Figure 15. - Percent airplane range increase due to combined effects of inlet location, jet cant for lift, and jet offset to avoid trim drag;  $c/t = 0.05$ .

~~CONFIDENTIAL~~

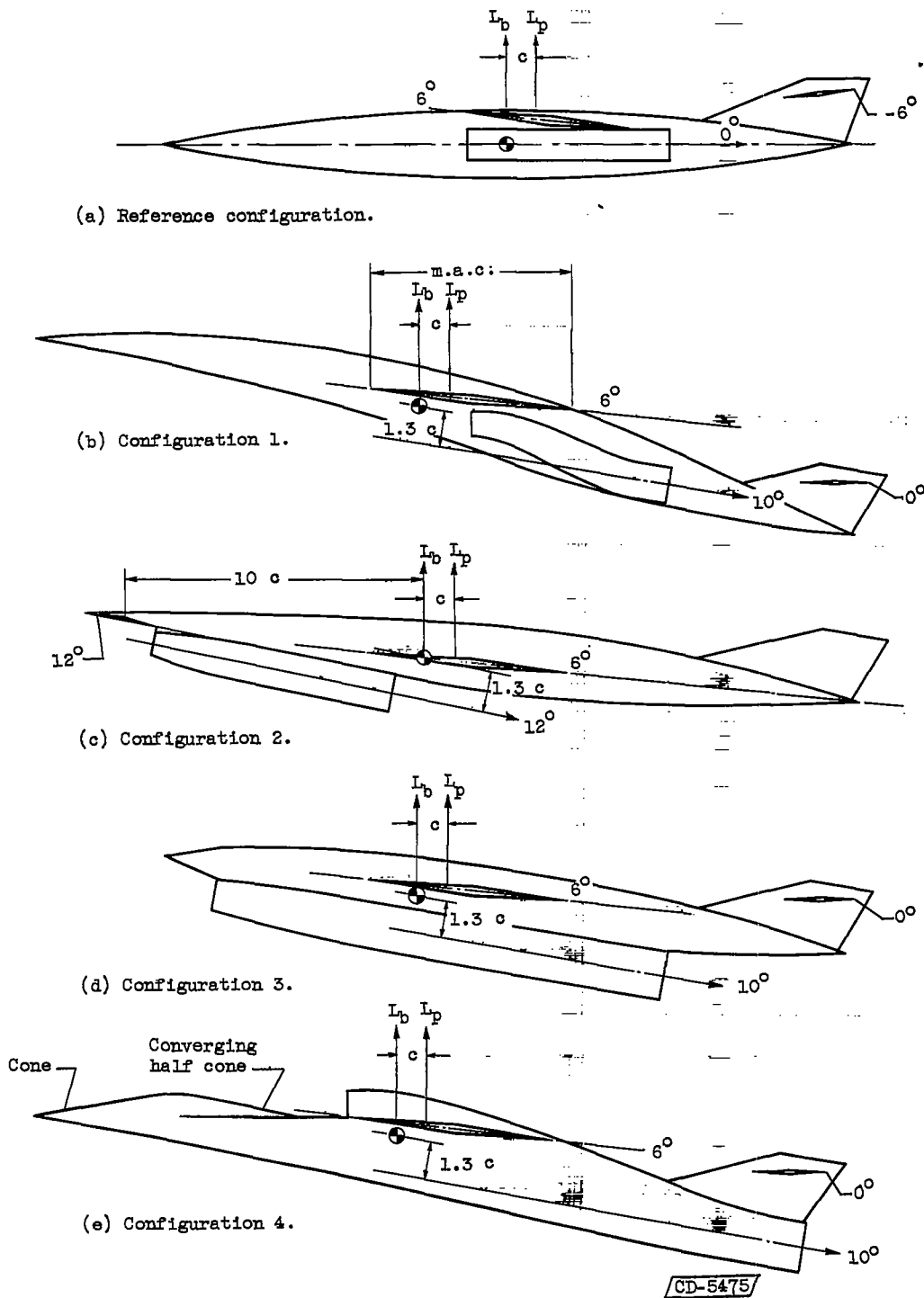


Figure 16. - Schematic airplane configurations incorporating inlet location for reduced inlet momentum and increased pressure recovery, jet cant for lift, and jet offset for avoiding trim drag. Flight Mach number, 4.0; engine cycle temperature, 3500° R; maximum airplane lift-drag ratio, 4;  $c$ , 0.15.

4077

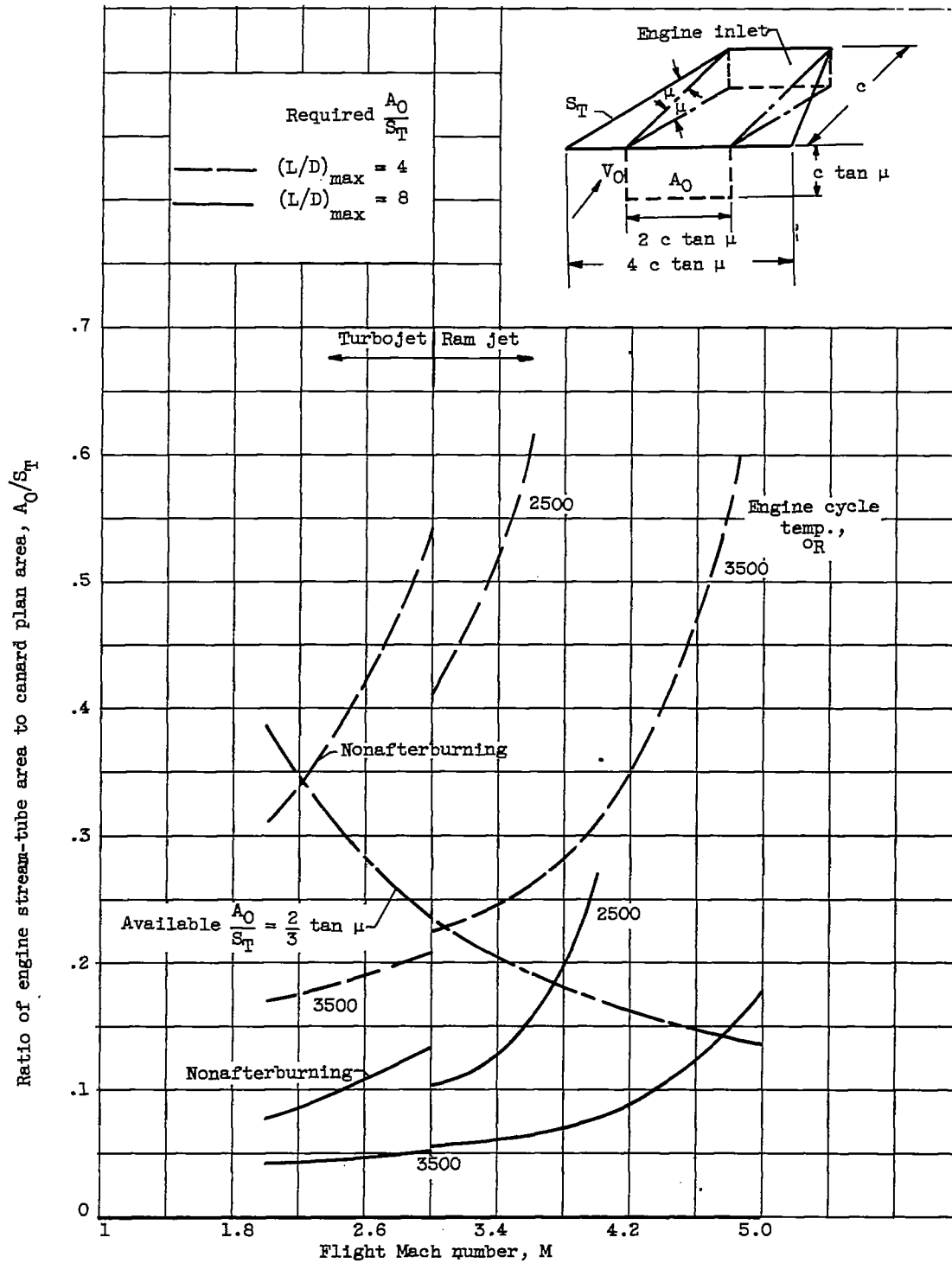
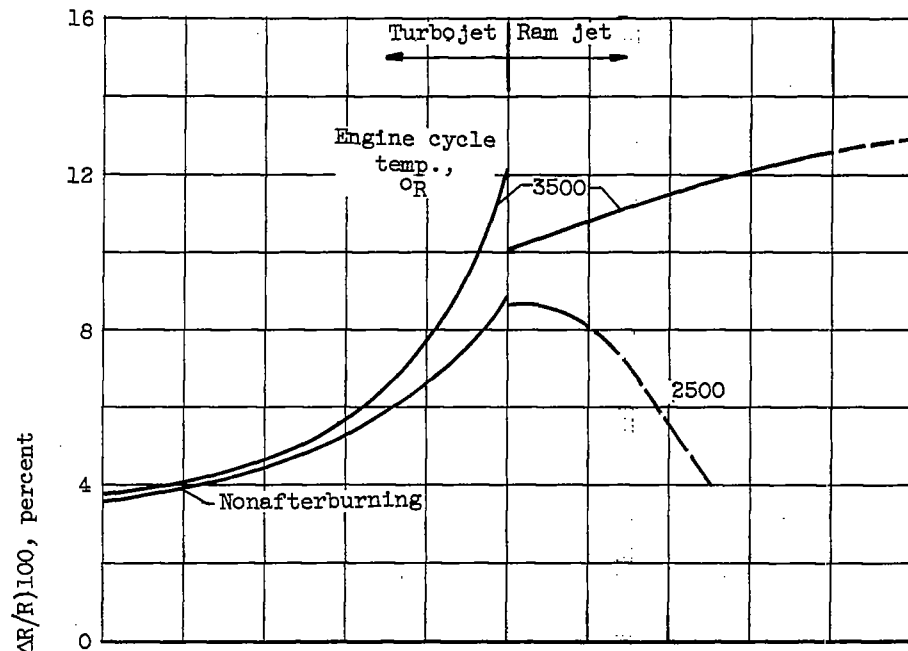
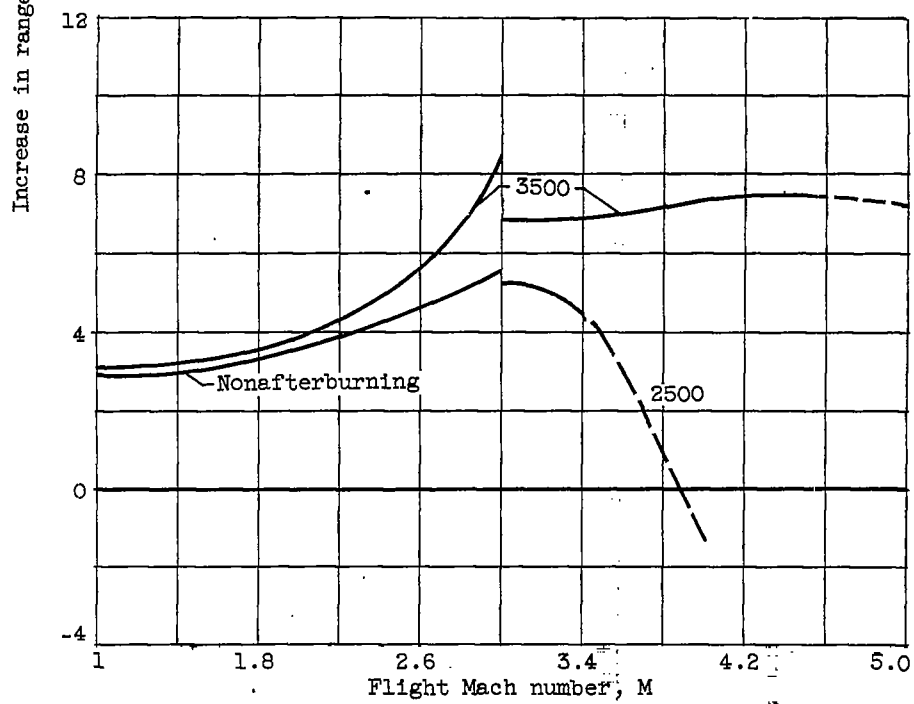


Figure 17. - Comparison of required ratio of engine-inlet stream-tube area to canard plan area with available area ratio;  $c/t = 0.10$ .



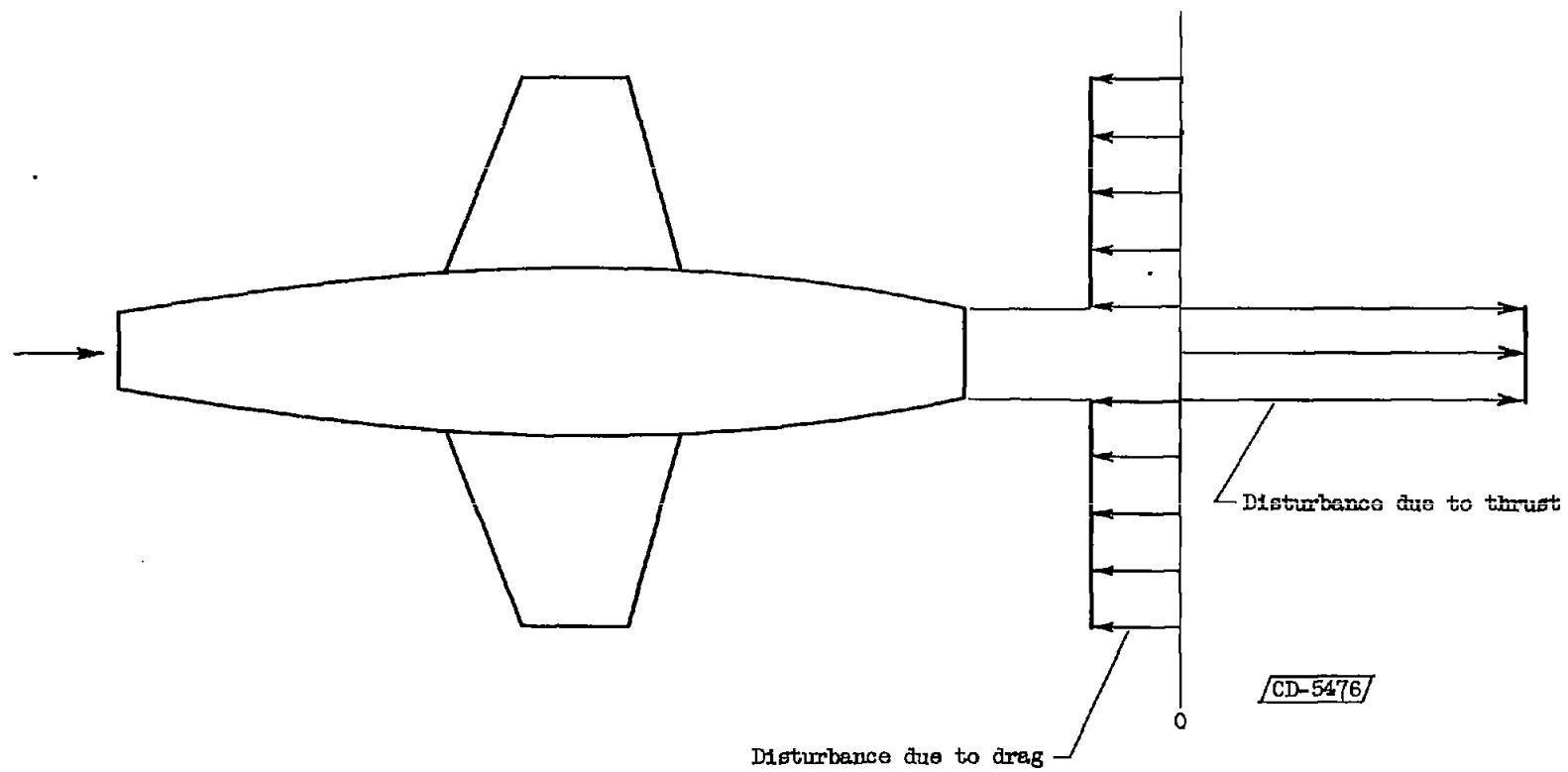
(a) Maximum airplane lift-drag ratio, 4.



(b) Maximum airplane lift-drag ratio, 8.

Figure 18. - Percent airplane range increase due to combined effects of inlet location and jet cant for trim;  $c/t$ , 0.05.

CONFIDENTIAL



CONFIDENTIAL

Figure 19. - Schematic velocity disturbance remaining in air behind an airplane.

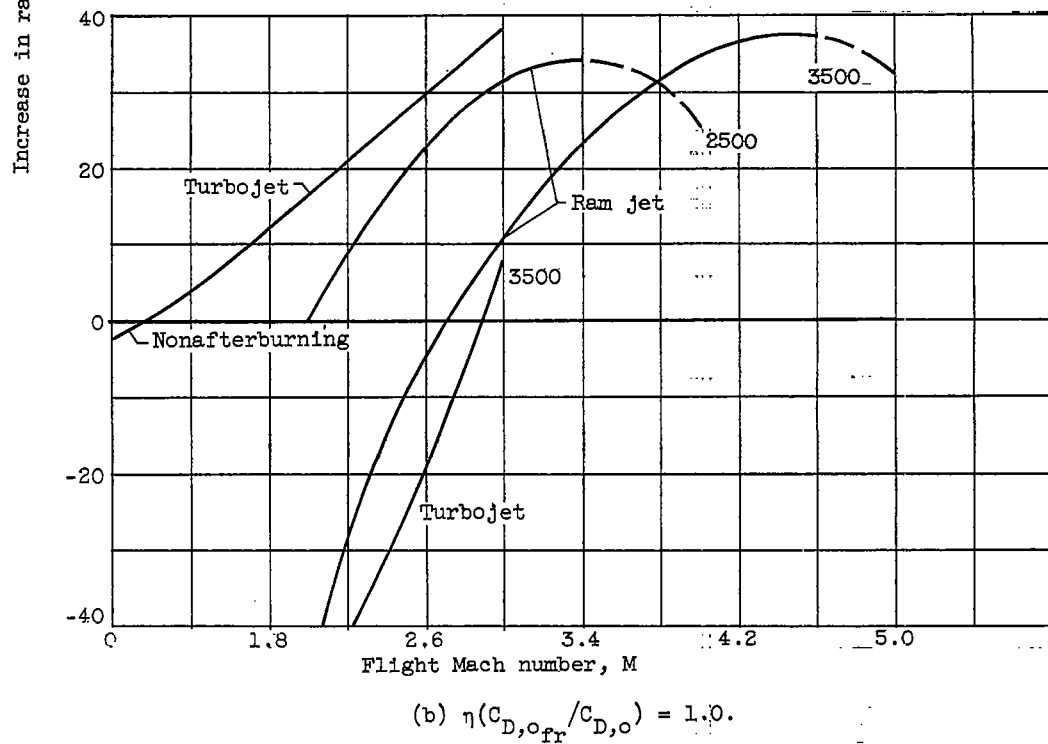
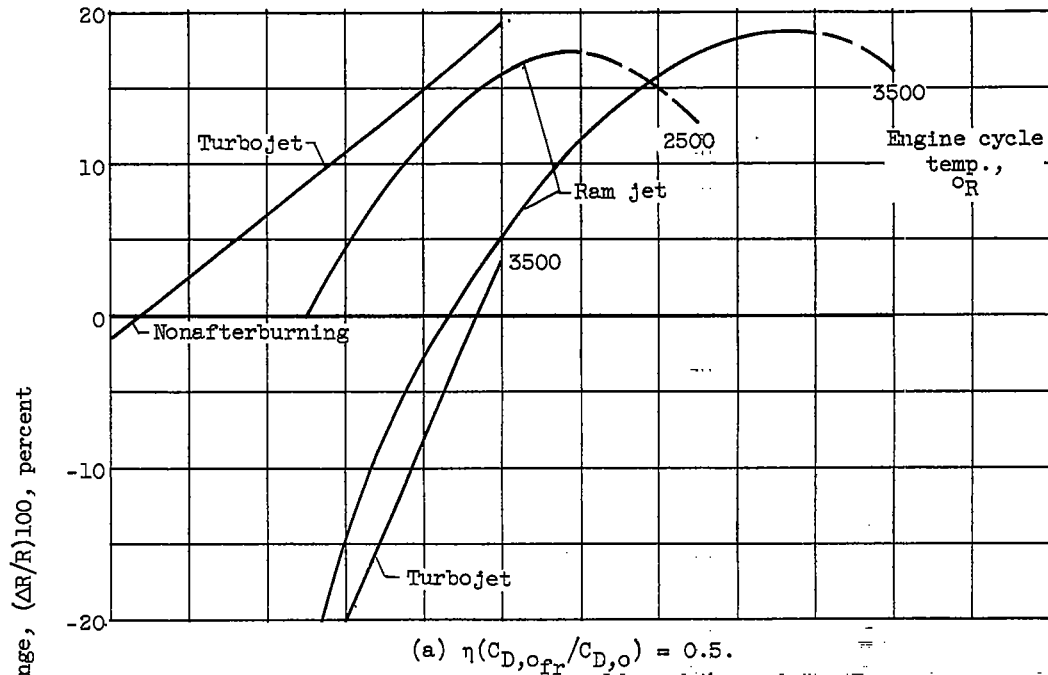
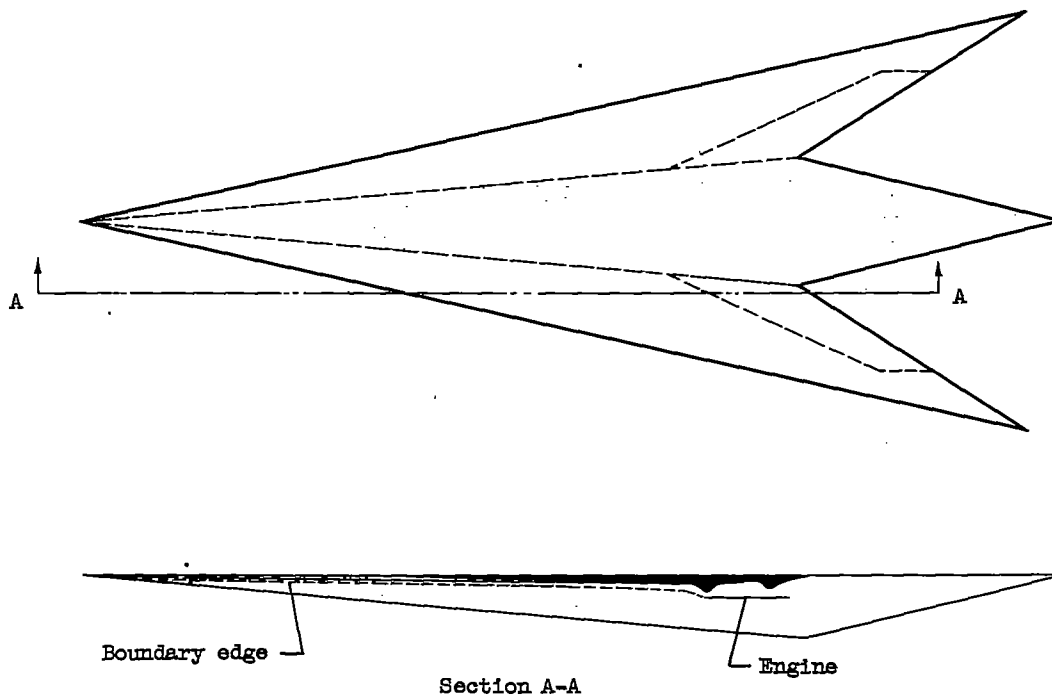


Figure 20. - Percent airplane range increase for using airframe boundary layer in engine cycle.



(a) Configuration A.



CD-5479

(b) Configuration B.

Figure 21. - Schematic airplane configuration incorporating use of boundary layer in engine.

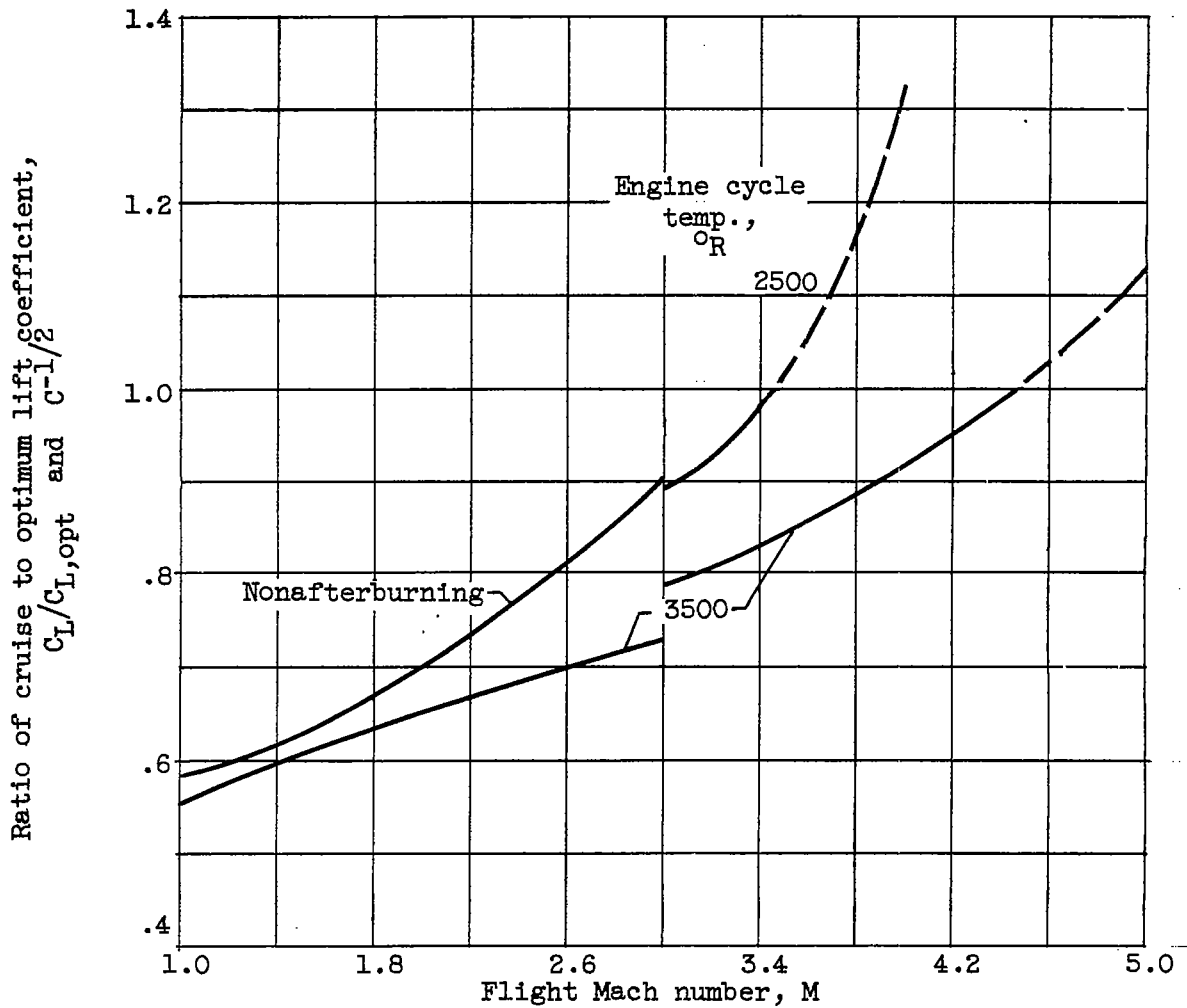


Figure 22. - Ratio of cruise to optimum lift coefficient (eq. (C2)).

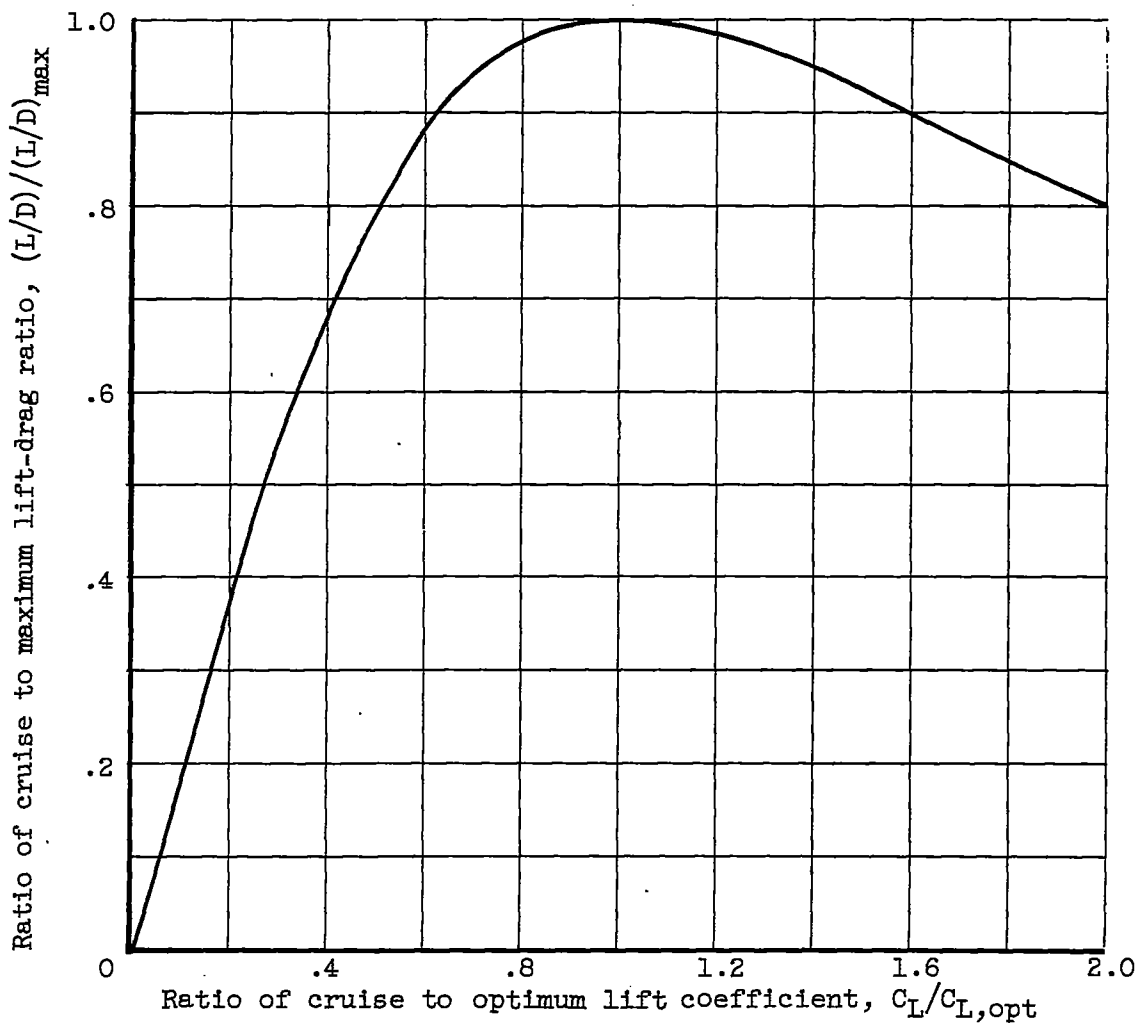


Figure 23. - Lift-drag ratio as function of lift coefficient (eq. (C16)).

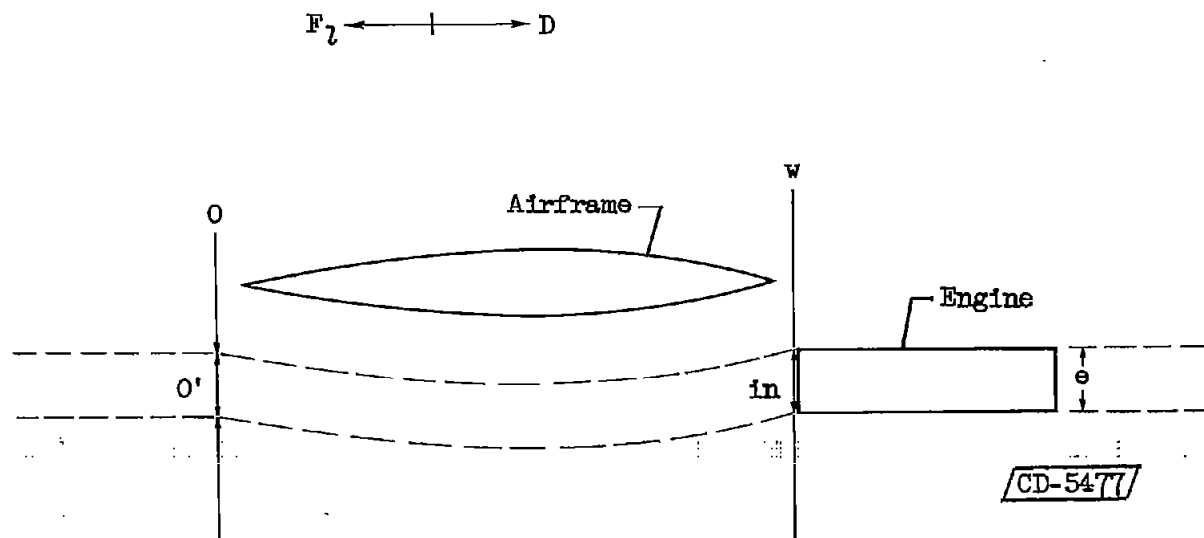


Figure 24. - Illustration of nomenclature related to engine and airframe.

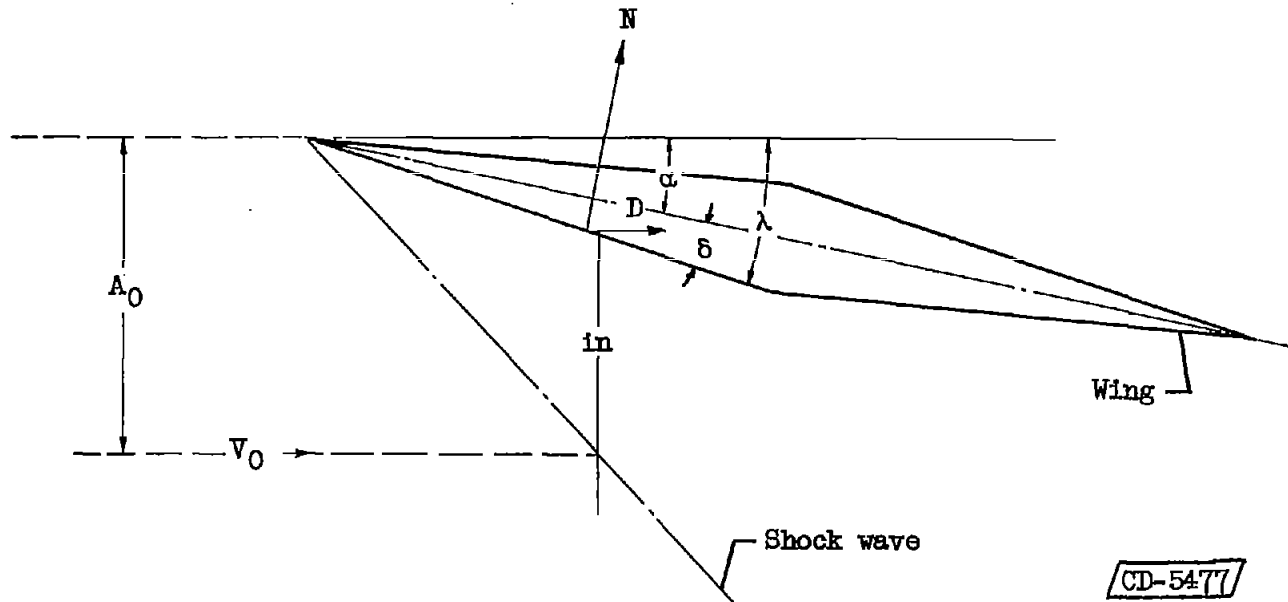


Figure 25. - Illustration of nomenclature related to wing.

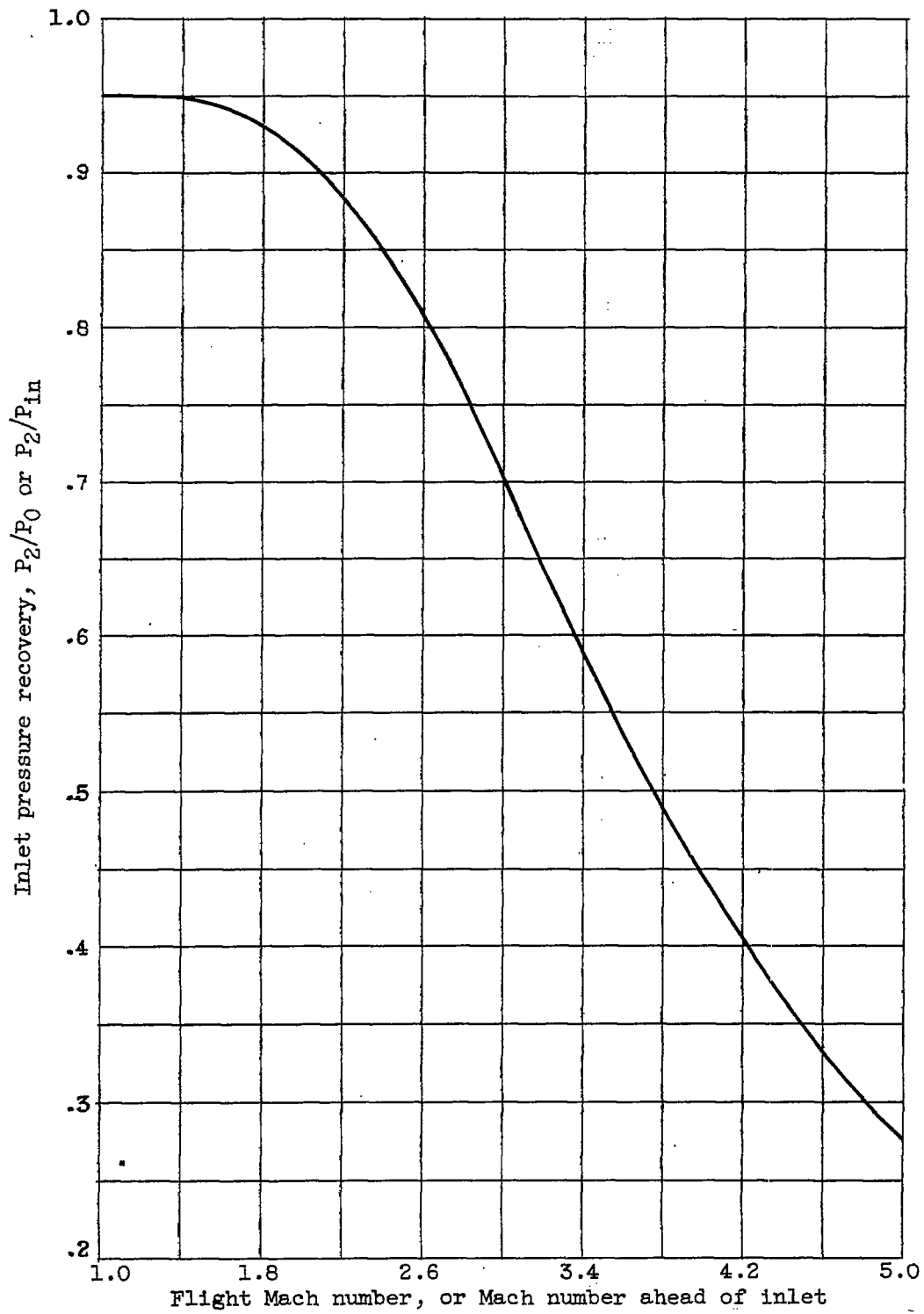


Figure 26. - Inlet pressure-recovery characteristics.

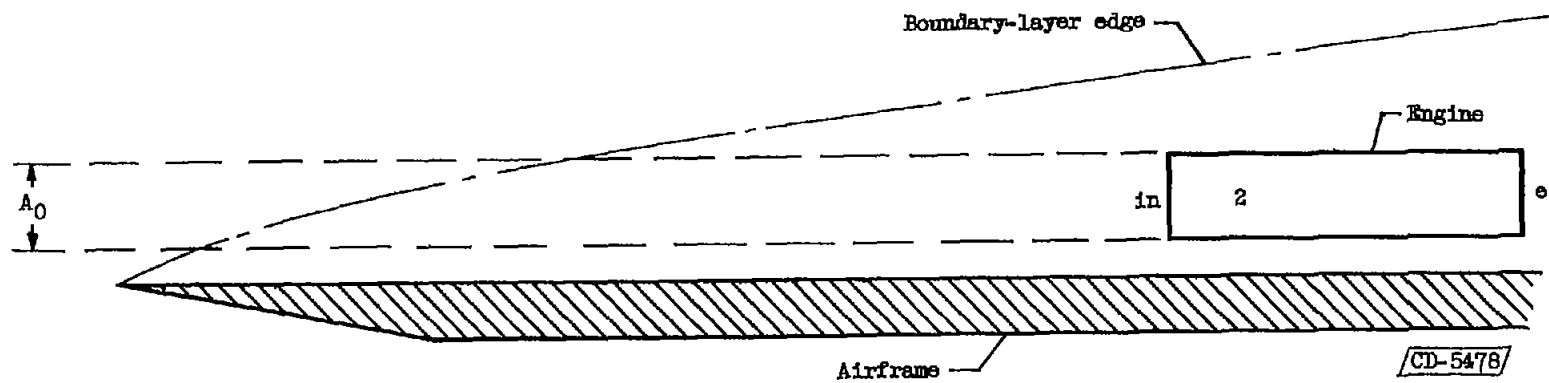


Figure 27. - Illustration of nomenclature related to use of boundary-layer air in engine.

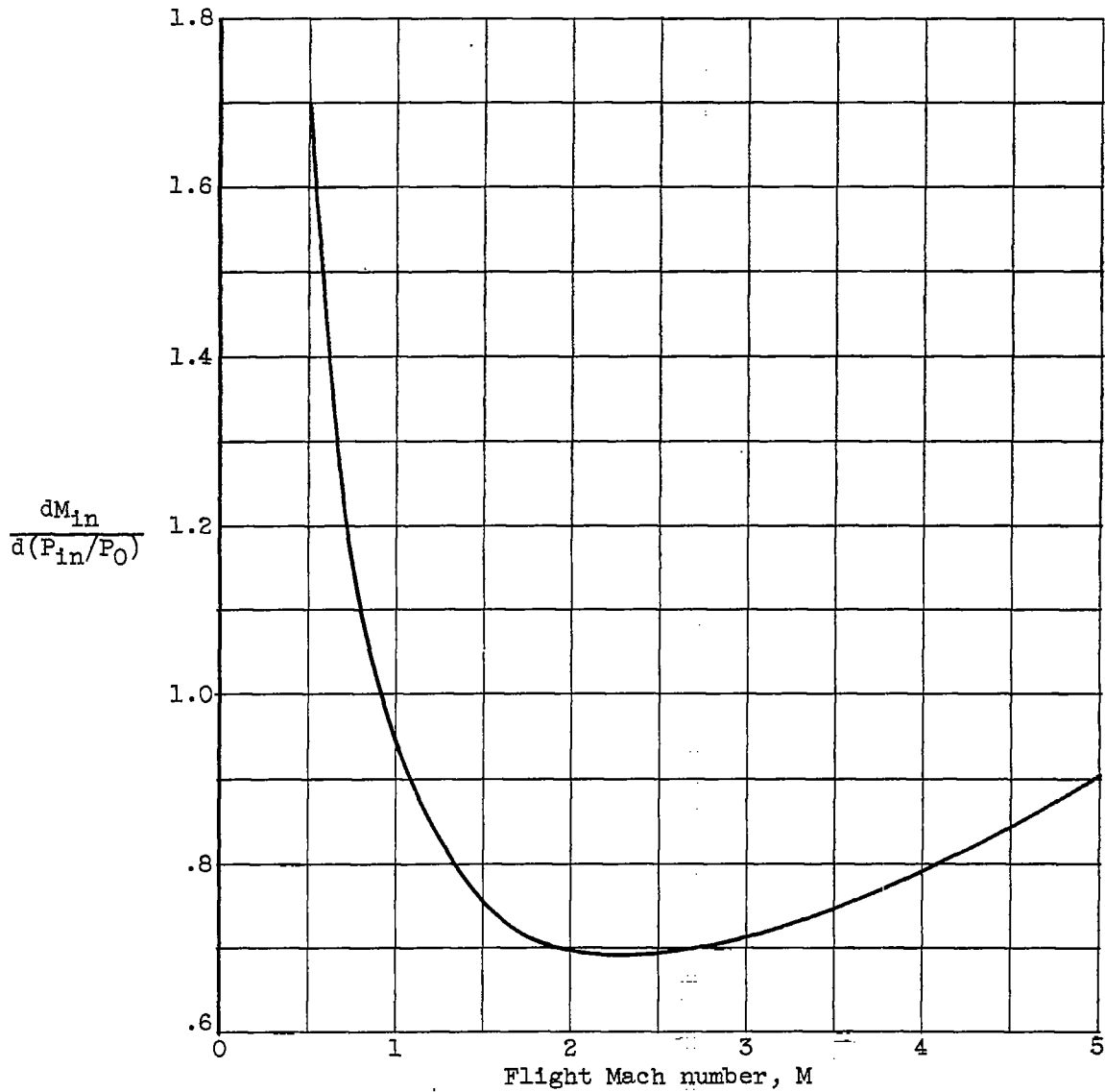


Figure 28. - Variation of  $\frac{dM_{in}}{d(P_{in}/P_0)}$  with Mach number.  
Stream static pressure and total temperature constant.